Vibro-acoustic characteristics analysis of the rotary composite plate and conical–cylindrical double cavities coupled system

Hong Zhang

College of Mechanical and Electrical Engineering,
Nanjing University of Aeronautics and Astronautics, Nanjing, China and
Jiangsu Key Laboratory of Precision and Micro-Manufacturing Technology,
Nanjing University of Aeronautics and Astronautics, Nanjing, China, and

Tianlin Chen

College of Mechanical and Electrical Engineering,
Nanjing University of Aeronautics and Astronautics, Nanjing, China

Abstract

Purpose – The purpose of the study is to obtain and analyze vibro-acoustic characteristics.

Design/methodology/approach – A unified analysis model for the rotary composite laminated plate and conical–cylindrical double cavities coupled system is established. The related parameters of the unified model are determined by isoparametric transformation. The modified Fourier series are applied to construct the admissible displacement function and the sound pressure tolerance function of the coupled systems. The energy functional of the structure domain and acoustic field domain is established, respectively, and the structure–acoustic coupling potential energy is introduced to obtain the energy functional. Rayleigh–Ritz method was used to solve the energy functional.

Findings – The displacement and sound pressure response of the coupled systems are acquired by introducing the internal point sound source excitation, and the influence of relevant parameters of the coupled systems is researched. Through research, it is found that the impedance wall can reduce the amplitude of the sound pressure response and suppress the resonance of the coupled systems. Besides, the composite laminated plate has a good noise reduction effect.

Originality/value – This study can provide the theoretical guidance for vibration and noise reduction.

Keywords Unified analysis model, Composite laminated plate, Rotary acoustic cavity, Plate-cavity coupled system, Vibro-acoustic characteristics

Paper type Research paper

1. Introduction

Rotary laminated plate structures based on fiber reinforced composite materials have been widely applied in aerospace, marine and other fields. In engineering practice, it is inevitable to produce the coupled system between rotary composite laminated plate and acoustic cavities.

Journal of Intelligent
Manufacturing and Special
Equipment
Vol. 3 No. 1, 2022
pp. 67-96
Emerald Publishing Limited
e-ISSN: 2633-660X
p-ISSN: 2633-6596
DOI 10.1108/JIMSE-01-2022-0002

Taking the submarine as an instance, the two cabins inside the hull of the submarine can be regarded as a rotary acoustic cavity coupled system, and the two cabins are separated by the cabin door composed of composite laminated plate. Noise in each cabin causes the variation of sound pressure, which leads to the vibration of the cabin door. Meanwhile, this vibration also contributes to noise, forming the composite laminated plate and double acoustic cavities coupled system. To compare the vibro-acoustic characteristics of structure–acoustic coupled system containing rotary composite laminated plate and acoustic cavity coupled system, it is important to conduct in-depth research on the vibro-acoustic characteristics of the rotary composite laminated plate and conical–cylindrical double acoustic cavities coupled system and reveal the vibro-acoustic coupling mechanism, which can provide the theoretical basis for structural optimization and low noise design.

The acoustic field characteristics of acoustic cavity coupled system under different conditions have been investigated by many scholars in recent years. Tanaka et al. (2012) derived the eigenpairs, which verified the validity by an experiment of coupled rectangular cavity, and investigated the fundamental properties of the eigenpairs derived. Moores et al. (2018) demonstrated an acoustical analog of a circuit quantum electrodynamics system that leverages acoustic properties to enable strong multimode coupling in the dispersive regime, and the operating frequencies where this emission rate is suppressed are identified. Unnikrishnan Nair et al. (2010) proposed a simplified modeling approach for numerical simulation of a coupled cavity-resonator system, and the influence of damping and resonator volume fraction on the coupled system performance is shown. A high-order doubly asymptotic open boundary for modeling scalar wave propagation in two-dimensional unbounded media was presented by Birk et al. (2016), which can handle domains with arbitrary geometry by using a circular boundary to divide these into near field and far field. Through modal energy analysis (MODENA), Zhang et al. (2016) defined a dimensionless coupling quotient, which is equal to the ratio of the gyroscopic coupling coefficient and the critical coefficient at modal frequencies. Chen et al. (2017) presented a domain decomposition method to predict the acoustic characteristics of an arbitrary enclosure made up of any number of sub-spaces and revealed the effect of coupling parameters between sub-spaces on the natural frequencies and mode shapes of the overall enclosure. Based on the energy principle in combination with a 3D modified Fourier cosine series approach, Shi et al. (2018) studied the modeling and acoustic eigen analysis of coupled spaces with a coupling aperture of variable size. It can be seen from the existing literature that the current research on acoustic cavity coupled system is mostly for rectangular cavity. However, the research on the acoustic characteristic model of the rotary acoustic cavity is rarely involved, let alone the research on the modeling of rotary acoustic cavity coupled system. At the same time, most of the investigations are based on the coupling mechanism analysis between acoustic cavities, while no analysis model has been established specifically.

Unlike the acoustic cavity coupled system, the coupling of rotary composite laminated plate and conical–cylindrical double acoustic cavities belongs to structure–acoustic coupling. Many scholars have researched the coupling mechanism of structure–sound coupled system. On the foundation of these investigations, the models of sectional structure–sound coupled system are established, and the vibro-acoustic characteristics of the coupled system are analyzed. Van Genechten et al. (2011) presented a newly developed hybrid simulation technique for coupled structural–acoustic analysis, which applies a wave-based model for the acoustic cavity and a direct or modally reduced finite element (FE) model for the structural part. By invoking the energy distribution approach, De Rosa et al. (2012) proposed a similitude for the analysis of the dynamic response of acoustic–elastic assemblies and discussed the FE modeling of a flexural plate coupled to an acoustic room and an infinite cylinder containing a fluid. Wang et al. (2015) developed a coupled smoothed finite element method (S-FEM) to deal with the structural–acoustic problems consisting of a shell

configuration interacting with the fluid medium; numerical examples of a cylinder cavity attached to a flexible shell and an automobile passenger compartment were conducted to illustrate the effectiveness and accuracy of the coupled S-FEM for structural–acoustic problems. Shu *et al.* (2014) proposed a level set-based structural topology optimization method for the optimal design of coupled structural–acoustic system with a focus on interior noise reduction. Some scholars have also studied the vibro-acoustic coupling characteristics of the composite laminated plate–double cavity coupled system and obtained some achievements. Larbi *et al.* (2012) demonstrated the theoretical formulation and the FE implementation of vibro-acoustic problems with piezoelectric composite structures connected to electric shunt circuits. Sarigül and Karagözlü (2014, 2018) presented the results of modal structure–sound coupling analysis for rectangular plates with different composite parameters and compared with the performance of isotropic plate systems. Ferreira *et al.* (2014), Carrera *et al.* (2018) and Cinefra *et al.* (2021) established a theoretical model of rectangular composite laminated plate and constructed a rectangular cavity model based on the FE formula of sound field under standard pressure. In the existing literature, the research object of the composite laminated plate-cavity coupled system is mostly concentrated on the rectangular composite laminated plate-cavity coupled system, while the rotary composite laminated plate-cavity coupled system is rarely studied, much less the rotary composite laminated plate and conical–cylindrical double acoustic cavities coupled system.
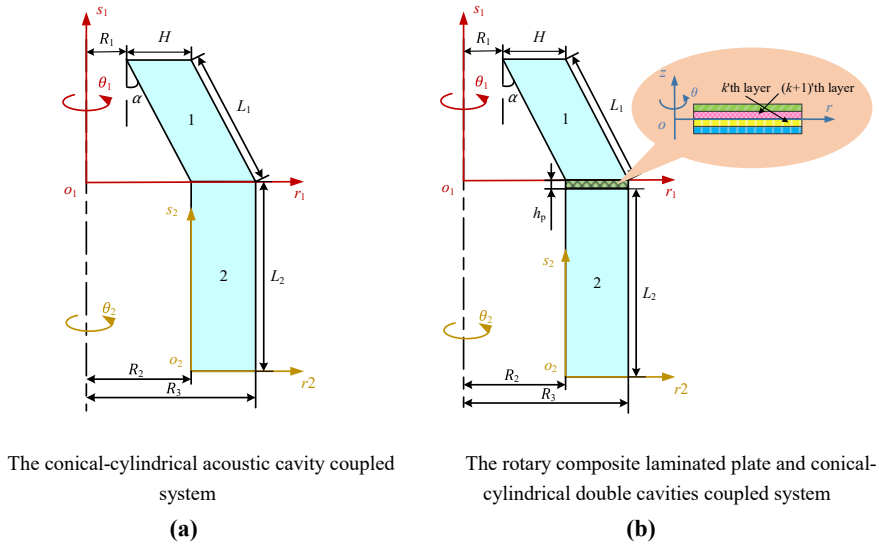
In view of the shortcomings of existing research, the vibro-acoustic characteristics analysis of the rotary composite laminated plate and conical–cylindrical double acoustic cavities coupled system are conducted in this paper. First, the expressions of admissible displacement function and sound pressure function of laminated plate are constructed. Second, the energy functional of the structure domain and sound field domain is established, respectively, and the coupling potential energy is added to acquire the energy functional of the whole coupled system. Then, Rayleigh–Ritz method is applied to gain the equation of the vibro-acoustic characteristics of the system. Finally, based on the fast convergence and accuracy of the model, the effect mechanism of relevant parameters on the vibro-acoustic characteristics is analyzed, and the response of the coupled system is investigated by introducing internal point force and point source excitation.

2. Unified analysis model of the coupled systems

2.1 Model description

Figure 1 demonstrates the rotating cross-section geometrical parameters and coordinate system of the conical–cylindrical acoustic cavity coupled system and rotary composite laminated plate and conical–cylindrical double cavities coupled system. As shown in Figure 1a, the coordinate of conical–cylindrical acoustic cavity coupled system is composed of two local coordinate systems $(o–s_1, \theta_1, r_1)$ and $(o–s_2, \theta_2, r_2)$. R_1 and R_2 separately represent the short radius and long radius of conical cavity 1, and α and L_1 are the cone-apex angle and the length of generatrix of conical cavity 1. R_2 and R_3 denote the inner radius and outer radius of cylindrical cavity 2, and the height of cylindrical cavity 2 is marked as L_1. Thickness of the acoustic cavity coupled system is represented as H. Compared with the coupled system in Figure 1a, the rotary composite laminated plate and conical–cylindrical double acoustic cavities coupled system add a composite plate between the two acoustic cavities. It can be found from Figure 1b that the coordinate of rotary composite laminated plate and conical–cylindrical double cavities coupled system is composed of three local coordinate systems $(o–s_1, \theta_1, r_1)$, $(o–s_2, \theta_2, r_2)$ and $(o–s_3, \theta_3, r_3)$. L_p is the thickness of composite laminated plate, and other geometric parameters have the same meanings as in Figure 1a. The shapes of rotary acoustic cavity coupled system at different rotation angles are given in Figure 2. The parameter ϑ is introduced here to express the rotation angles of coupled systems, and

Figure 1.
Cross-section geometrical parameters and coordinate system of the coupled systems

The conical-cylindrical acoustic cavity coupled system

(a)

The rotary composite laminated plate and conical-cylindrical double cavities coupled system

(b)

whether rotation angles are 2π is related to the number of acoustic walls in the coupled systems. In order to study the vibro-acoustic characteristics of the coupled systems, a monopole point sound source Q is placed.

In Figure 3, the general boundary conditions on the edge of rotary composite laminated plate are represented by introducing three groups of linear springs k_u, k_v, k_w along u, v, w directions and two groups of torsion springs K_r and K_θ, which are continuously distributed along the boundary. u, v and w denote r, θ and s directions, respectively. $k_{\theta 0}^u$, $k_{\theta 0}^v$, $k_{\theta 0}^w$, $K_{\theta 0}^r$ and $K_{\theta 0}^\theta$ are introduced to represent the five groups of boundary springs at the boundary $\theta = 0$, and the boundary springs at $\theta = \vartheta$, $r = 0$ and $r = H$ can also be expressed in a similar way. When the rotation angle $\vartheta = 2\pi$, the coupling boundary shown in Figure 3b is generated for the rotary composite laminated plate. Three groups of linear coupling springs k_{uc}, k_{vc} and k_{wc} and two groups of torsion springs K_{rc} and $K_{\theta c}$ are uniformly set on the coupling boundary ($\theta = 0$ and $\theta = 2\pi$). Therefore, the coupling of the rotating composite laminated plate can be realized.

2.2 Related parameter of unified model
To ensure that the systems can be coupled during the modeling process, the parallelogram section in conical acoustic cavity is necessary to be transformed into a square section. It can be found from Figure 4 that the plane *ros* coordinate system is transformed to plane $\xi o\eta$ coordinate system by iso-parametric transformation, where each vertex in plane $\xi o\eta$ coordinate system has been determined as (0, 0), (1, 0), (1, 1) and (0, 1).

Using the four-node coordinate transformation in the FE method, the coordinate transformation equations are as follows:

$$\begin{Bmatrix} r \\ s \end{Bmatrix} = \sum_{i=1}^{4} N_i(\xi, \eta) \begin{Bmatrix} r_{(i)} \\ s_{(i)} \end{Bmatrix} \tag{1}$$

$$N_i(\xi, \eta) = (-1)^{i+1} \left(1 - \xi_{(i)} - \xi\right)\left(1 - \eta_{(i)} - \eta\right) \tag{2}$$

Figure 2.
Unified model of the
coupled systems

in which $(r_{(i)}, s_{(i)})$ and $(\xi_{(i)}, \eta_{(i)})$ separately denote the coordinate of the ith vertex in the plane ros coordinate system and plane $\xi o\eta$ coordinate system, and $N_i(\xi, \eta)$ is the shape function of the ith vertex of the plane ros coordinate system.
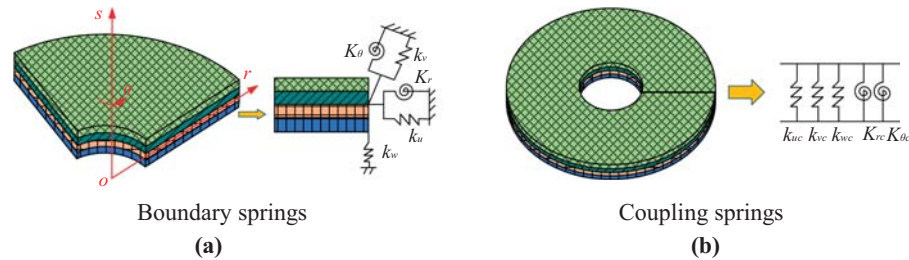
The specific coordinate system transformation process is expressed in the matrix form:

$$\left[\frac{\partial}{\partial \xi} \quad \frac{\partial}{\partial \eta} \right]^{\mathrm{T}} = J \left[\frac{\partial}{\partial r} \quad \frac{\partial}{\partial s} \right]^{\mathrm{T}} \tag{3}$$

$$J = \begin{bmatrix} \dfrac{\partial r}{\partial \xi} & \dfrac{\partial s}{\partial \xi} \\ \dfrac{\partial r}{\partial \eta} & \dfrac{\partial s}{\partial \eta} \end{bmatrix} \tag{4}$$

where

$$\begin{cases} \dfrac{\partial r}{\partial \xi} = \dfrac{\partial \left[\sum\limits_{i=1}^{4} N_i(\xi,\eta) r_{(i)} \right]}{\partial \xi} \\[4mm] \dfrac{\partial r}{\partial \eta} = \dfrac{\partial \left[\sum\limits_{i=1}^{4} N_i(\xi,\eta) r_{(i)} \right]}{\partial \eta} \end{cases} \quad \begin{cases} \dfrac{\partial s}{\partial \xi} = \dfrac{\partial \left[\sum\limits_{i=1}^{4} N_i(\xi,\eta) s_{(i)} \right]}{\partial \xi} \\[4mm] \dfrac{\partial s}{\partial \eta} = \dfrac{\partial \left[\sum\limits_{i=1}^{4} N_i(\xi,\eta) s_{(i)} \right]}{\partial \eta} \end{cases} \tag{5}$$

Figure 3.
The boundary springs and coupled springs of the rotary composite laminated plate

Boundary springs
(a)

Coupling springs
(b)

Figure 4.
Schematic diagram of coordinate transformation of parallelogram section

Equation (3) is frequently expressed in the inverse form:

$$\left[\frac{\partial}{\partial r} \quad \frac{\partial}{\partial s}\right]^{\mathrm{T}} = J^{-1}\left[\frac{\partial}{\partial \xi} \quad \frac{\partial}{\partial \eta}\right]^{\mathrm{T}} \tag{6}$$

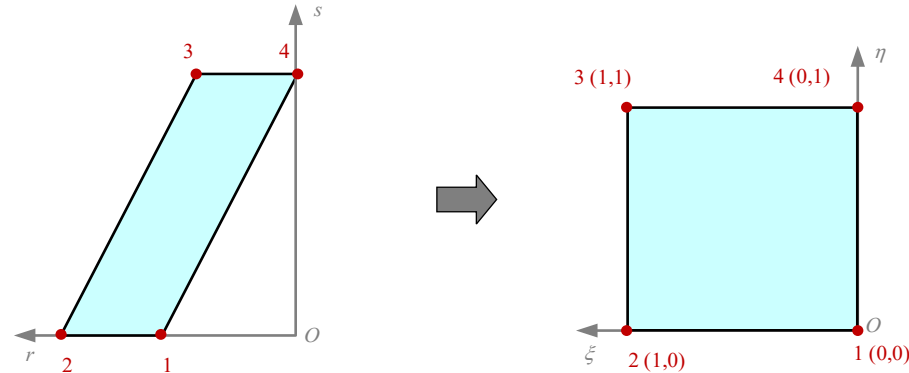$$J^{-1} = \begin{bmatrix} J_{11} & J_{12} \\ J_{21} & J_{22} \end{bmatrix} = \frac{1}{|J|}\begin{bmatrix} \dfrac{\partial s}{\partial \eta} & -\dfrac{\partial s}{\partial \xi} \\ -\dfrac{\partial r}{\partial \eta} & \dfrac{\partial r}{\partial \xi} \end{bmatrix} \tag{7}$$

where $|J|$ is the determinant of the Jacobian matrix.

Table 1 shows the related parameters between the local coordinate systems of conical and cylindrical acoustic cavity and the coordinate system of double curvature cavity element (α, β, z). In addition, the Lame coefficient of the cavity and the value range of the corresponding coordinate axis are also given:

2.3 Construction of admissible displacement and sound pressure functions
Based on the first-order shear deformation theory (FSDT) and two-dimensional modified Fourier series theory, the admissible displacement function of rotary composite laminated plate is established. The admissible sound pressure functions of conical and cylindrical cavities are constructed by three-dimensional modified Fourier series. The expression is the superposition of a cosine function and six sines and cosines functions. The specific expressions can be written as follows (Zhang *et al.*, 2019, 2020a, b):

$$u(r, \theta, t) = e^{-j\omega t}\left(\mathbf{\Phi}_u^{\mathrm{M}}(r, \theta) + \sum_{N_q=1}^{2} \mathbf{\Phi}_u^{N_q}(r, \theta)\right)\mathbf{A}_{mn} \tag{8}$$

$$v(r, \theta, t) = e^{-j\omega t}\left(\mathbf{\Phi}_v^{\mathrm{M}}(r, \theta) + \sum_{N_q=1}^{2} \mathbf{\Phi}_v^{N_q}(r, \theta)\right)\mathbf{B}_{mn} \tag{9}$$

$$w(r, \theta, t) = e^{-j\omega t}\left(\mathbf{\Phi}_w^{\mathrm{M}}(r, \theta) + \sum_{N_q=1}^{2} \mathbf{\Phi}_w^{N_q}(r, \theta)\right)\mathbf{C}_{mn} \tag{10}$$

Cavity type	Related parameter Parameter type	Specific parameter
Conical acoustic cavity	Coordinate relation	$\alpha_1 = \eta_1, \beta_1 = \theta_1 z_1 = \xi_1$
	Transformation	$|J_1| = L_1 H \cos\alpha, J_{11}^1 = 1/H, J_{21}^1 = \tan\alpha/H, J_{12}^1 = 0,$ $J_{22}^1 = 1/L_1 \cdot \cos\alpha$
	Lame coefficient	$H_{\alpha_1} = 1, H_{\beta_1} = r_1 = R_2 + (R_1 - R_2)\cdot\eta + H\cdot\xi, H_{z_1} = 1$
	Value range	$0 \leq L_{\alpha_1} \leq 1, 0 \leq L_{\beta_1} \leq \vartheta_1, 0 \leq L_{z_1} \leq 1$
Cylindrical acoustic cavity	Coordinate relation	$\alpha_2 = s_2, \beta_2 = \theta_2, z_2 = r_2$
	Transformation	$|J_2| = 1, J_{11}^2 = J_{22}^2 = \sqrt{2}/2, J_{12}^2 = J_{21}^2 = 0$
	Lame coefficient	$H_{\alpha_2} = 1, H_{\beta_2} = r_2, H_{z_2} = 1$
	Value range	$0 \leq L_{\alpha_2} \leq L_2, 0 \leq L_{\beta_2} \leq \vartheta_2, 0 \leq L_{z_2} \leq H$

Table 1.
Parameters related to conversion between rotary acoustic cavities

$$\phi_r(r,\theta,t) = e^{-j\omega t}\left(\mathbf{\Phi}_{\phi_r}^{\mathrm{M}}(r,\theta) + \sum_{\mathrm{N}_q=1}^{2}\mathbf{\Phi}_{\phi_r}^{\mathrm{N}_q}(r,\theta)\right)\mathbf{D}_{mn} \tag{11}$$

$$\phi_\theta(r,\theta,t) = e^{-j\omega t}\left(\mathbf{\Phi}_{\phi_\theta}^{\mathrm{M}}(r,\theta) + \sum_{\mathrm{N}_q=1}^{2}\mathbf{\Phi}_{\phi_\theta}^{\mathrm{N}_q}(r,\theta)\right)\mathbf{E}_{mn} \tag{12}$$

$$p_1(r_1,\theta_1,s_1,t) = e^{-j\omega t}\left(\mathbf{P}_1^{\Omega}(r_1,\theta_1,s_1) + \sum_{\Theta_q=1}^{6}\mathbf{P}_1^{\Theta_q}(r_1,\theta_1,s_1)\right)\mathbf{F}_{m_t n_t l_t} \tag{13}$$

$$p_2(r_2,\theta_2,s_2,t) = e^{-j\omega t}\left(\mathbf{P}_2^{\Omega}(r_2,\theta_2,s_2) + \sum_{\Theta_q=1}^{6}\mathbf{P}_2^{\Theta_q}(r_2,\theta_2,s_2)\right)\mathbf{G}_{m_t n_t l_t} \tag{14}$$

in which $u\,(r,\theta,t)$, $v\,(r,\theta,t)$ and $w\,(r,\theta,t)$ separately represent the admissible displacement function of the surface in the r, θ and z directions of the rotary composite laminated plate, and $\phi_r(r,\theta,t)$ and $\phi_\theta(r,\theta,t)$ denote the lateral rotation in the r and θ directions, respectively. p_n ($n = 1, 2$) is the expression of the admissible sound pressure function for the nth cavity in the coupled system. The displacement supplement polynomials of rotary composite laminated plate can be expressed as $\mathbf{\Phi}^{\mathrm{M}}$ and $\mathbf{\Phi}^{\mathrm{N}_q}$ ($\mathrm{N}_q = 1, 2$), and the sound pressure supplement polynomials of the nth cavity are written as $\mathbf{P}_n^{\Omega}$ and $\mathbf{P}_n^{\Theta_q}$ ($\mathbf{\Theta}_q = 1, 2, \ldots, 6$). While $\mathbf{A}_{mn}$, $\mathbf{B}_{mn}$, $\mathbf{C}_{mn}$, $\mathbf{D}_{mn}$ and $\mathbf{E}_{mn}$ represent the unknown two-dimensional Fourier coefficient vectors and unknown three-dimensional Fourier coefficient vectors. These parameters can be expressed as follows:

$$\mathbf{\Phi}_u^{\mathrm{M}} = \mathbf{\Phi}_w^{\mathrm{M}} = \mathbf{\Phi}_v^{\mathrm{M}} = \mathbf{\Phi}_{\phi_r}^{\mathrm{M}} = \mathbf{\Phi}_{\phi_\theta}^{\mathrm{M}} = \mathbf{\Phi}^{\mathrm{M}} = \left\{\begin{array}{l}\cos\lambda_0^{\alpha}r\cos\lambda_0^{\beta}\theta, \cdots, \cos\lambda_0^{\alpha}r\cos\lambda_n^{\beta}\theta, \cdots, \\ \cos\lambda_0^{\alpha}r\cos\lambda_N^{b}\theta, \cdots, \cos\lambda_M^{\alpha}r\cos\lambda_N^{\beta}\theta\end{array}\right\} \tag{15}$$

$$\mathbf{\Phi}_u^{\mathrm{N}_1} = \mathbf{\Phi}_v^{\mathrm{N}_1} = \mathbf{\Phi}_w^{\mathrm{N}_1} = \mathbf{\Phi}_{\phi_r}^{\mathrm{N}_1} = \mathbf{\Phi}_{\phi_\theta}^{\mathrm{N}_1} = \left\{\begin{array}{l}\sin\left(\lambda_{-2}^{\alpha}r\right)\cos\left(\lambda_0^{\beta}\theta\right), \cdots, \sin\left(\lambda_{-2}^{\alpha}r\right)\cos\left(\lambda_n^{\beta}\theta\right), \cdots, \\ \sin\left(\lambda_{-2}^{\alpha}r\right)\cos\left(\lambda_N^{\beta}\theta\right), \cdots, \sin\left(\lambda_{-1}^{\alpha}r\right)\cos\left(\lambda_N^{\beta}\theta\right)\end{array}\right\} \tag{16}$$

$$\mathbf{\Phi}_u^{\mathrm{N}_2} = \mathbf{\Phi}_v^{\mathrm{N}_2} = \mathbf{\Phi}_w^{\mathrm{N}_2} = \mathbf{\Phi}_{\phi_r}^{\mathrm{N}_2} = \mathbf{\Phi}_{\phi_\theta}^{\mathrm{N}_2} == \left\{\begin{array}{l}\cos\left(\lambda_0^{\alpha}r\right)\sin\left(\lambda_{-2}^{\beta}\theta\right), \cos\left(\lambda_0^{\alpha}r\right)\sin\left(\lambda_{-1}^{\beta}\theta\right), \cdots, \\ \cos\left(\lambda_m^{\alpha}r\right)\sin\left(\lambda_{-2}^{\beta}\theta\right), \cdots, \cos\left(\lambda_M^{\alpha}r\right)\sin\left(\lambda_{-1}^{\beta}\theta\right)\end{array}\right\} \tag{17}$$

$$\mathbf{P}_n^{\Omega}(r_n,\theta_n,s_n) = \left\{\begin{array}{l}\cos\lambda_0^{\alpha_n}r_n\cos\lambda_0^{\beta_n}\theta_n\cos\lambda_0^{z_n}s_n, \cdots, \cos\lambda_0^{\alpha_n}r_n\cos\lambda_0^{\beta_n}\theta_n\cos\lambda_{L_c}^{z_n}s_n, \cdots, \\ \cos\lambda_0^{\alpha_n}r_n\cos\lambda_{N_c}^{\beta_n}\theta_n\cos\lambda_{L_c}^{z_n}s_n, \cdots, \cos\lambda_{M_c}^{\alpha_n}r_n\cos\lambda_{N_c}^{\beta_n}\theta_n\cos\lambda_{L_c}^{z_n}s_n\end{array}\right\} \tag{18}$$

$$\mathbf{P}_n^{\Theta_1}(r_n,\theta_n,s_n) = \left\{\begin{array}{l}\sin\lambda_{-2}^{\alpha_n}r_n\cos\lambda_0^{\beta_n}\theta_n\cos\lambda_0^{z_n}s_n, \cdots, \sin\lambda_{-2}^{\alpha_n}r_n\cos\lambda_0^{\beta_n}\theta_n\cos\lambda_{L_c}^{z_n}s_n, \cdots, \\ \sin\lambda_{-2}^{\alpha_n}r_n\cos\lambda_{N_c}^{\beta_n}\theta_n\cos\lambda_{L_c}^{z_n}s_n, \cdots, \sin\lambda_{-1}^{\alpha_n}r_n\cos\lambda_{N_c}^{\beta_n}\theta_n\cos\lambda_{L_c}^{z_n}s_n\end{array}\right\} \tag{19}$$

$$\mathbf{P}_n^{\Theta_2}(r_n,\theta_n,s_n) = \left\{\begin{array}{l}\cos\lambda_0^{\alpha_n}r_n\sin\lambda_{-2}^{\beta_n}\theta_n\cos\lambda_0^{z_n}s_n, \cdots, \cos\lambda_0^{\alpha_n}r_n\sin\lambda_{-2}^{\beta_n}\theta_n\cos\lambda_{L_c}^{z_n}s_n, \cdots, \\ \cos\lambda_0^{\alpha_n}r_n\sin\lambda_{-2}^{\beta_n}\theta_n\cos\lambda_{L_c}^{z_n}s_n, \cdots, \cos\lambda_{M_c}^{\alpha_n}r_n\sin\lambda_{-1}^{\beta_n}\theta_n\cos\lambda_{L_c}^{z_n}s_n\end{array}\right\} \tag{20}$$

$$\mathbf{P}_n^{\Theta_3}(r_n,\theta_n,s_n) = \left\{\begin{array}{l}\cos\lambda_0^{\alpha_n}r_n\cos\lambda_0^{\beta_n}\theta_n\sin\lambda_{-2}^{z_n}s_n, \cos\lambda_0^{\alpha_n}r_n\cos\lambda_0^{\beta_n}\theta_n\sin\lambda_{-1}^{z_n}s_n, \cdots, \\ \cos\lambda_0^{\alpha_n}r_n\cos\lambda_{N_c}^{\beta_n}\theta_n\sin\lambda_{-2}^{z_n}s_n, \cdots, \cos\lambda_{M_c}^{\alpha_n}r_n\cos\lambda_{N_c}^{\beta_n}\theta_n\sin\lambda_{-1}^{z_n}s_n\end{array}\right\} \tag{21}$$

$$\mathbf{P}_n^{\Theta_4}(r_n,\theta_n,s_n) = \left\{ \begin{array}{l} \sin\lambda_{-2}^{\alpha_n}r_n\sin\lambda_{-2}^{\beta_n}\theta_n\cos\lambda_0^{z_n}s_n,\cdots,\sin\lambda_{-2}^{\alpha_n}r_n\sin\lambda_{-2}^{\beta_n}\theta_n\cos\lambda_{L_c}^{z_n}s_n,\cdots, \\ \sin\lambda_{-2}^{\alpha_n}r_n\cos\lambda_{-1}^{\beta_n}\theta_n\cos\lambda_{L_c}^{z_n}s_n,\cdots,\sin\lambda_{-1}^{\alpha_n}r_n\cos\lambda_{-1}^{\beta_n}\theta_n\cos\lambda_{L_c}^{z_n}s_n \end{array} \right\} \quad (22)$$

$$\mathbf{P}_n^{\Theta_5}(r_n,\theta_n,s_n) = \left\{ \begin{array}{l} \sin\lambda_{-2}^{\alpha_n}r_n\cos\lambda_0^{\beta_n}\theta_n\sin\lambda_{-2}^{z_n}s_n,\sin\lambda_{-2}^{\alpha_n}r_n\cos\lambda_0^{\beta_n}\theta_n\sin\lambda_{-1}^{z_n}s_n,\cdots, \\ \sin\lambda_{-2}^{\alpha_n}r_n\cos\lambda_{N_c}^{\beta_n}\theta_n\sin\lambda_{-2}^{z_n}s_n,\cdots,\sin\lambda_{-1}^{\alpha_n}r_n\cos\lambda_{N_c}^{\beta_n}\theta_n\sin\lambda_{-1}^{z_n}s_n \end{array} \right\} \quad (23)$$

$$\mathbf{P}_n^{\Theta_6}(r_n,\theta_n,s_n) = \left\{ \begin{array}{l} \cos\lambda_0^{\alpha_n}r_n\sin\lambda_{-2}^{\beta_n}\theta_n\sin\lambda_{-2}^{z_n}s_n,\cos\lambda_0^{\alpha_n}r_n\sin\lambda_{-2}^{\beta_n}\theta_n\cos\lambda_{-1}^{z_n}s_n,\cdots, \\ \cos\lambda_0^{\alpha_n}r_n\sin\lambda_{-1}^{\beta_n}\theta_n\sin\lambda_{-2}^{z_n}s_n,\cdots,\cos\lambda_{M_c}^{\alpha_n}r_n\sin\lambda_{-1}^{\beta_n}\theta_n\cos\lambda_{-1}^{z_n}s_n \end{array} \right\} \quad (24)$$

$$\mathbf{A}_{mn} = \left\{ \begin{array}{l} A_{0,0}^1,\cdots,A_{0,n}^1,\cdots,A_{m,n}^1,\cdots,A_{M,N}^1,A_{-2,0}^2,\cdots,A_{-2,n}^2,\cdots, \\ A_{-2,N}^2,\cdots,A_{-1,N}^2,A_{0,-2}^3,A_{0,-1}^3,\cdots,A_{m,-2}^3,\cdots,A_{M,-1}^3 \end{array} \right\}^T \quad (25)$$

$$\mathbf{B}_{mn} = \left\{ \begin{array}{l} B_{0,0}^1,\cdots,B_{0,n}^1,\cdots,B_{m,n}^1,\cdots,B_{M,N}^1,B_{-2,0}^2,\cdots,B_{-2,n}^2,\cdots, \\ B_{-2,N}^2,\cdots,B_{-1,N}^2,B_{0,-2}^3,B_{0,-1}^3,\cdots,B_{m,-2}^3,\cdots,B_{M,-1}^3 \end{array} \right\}^T \quad (26)$$

$$\mathbf{C}_{mn} = \left\{ \begin{array}{l} C_{0,0}^1,\cdots,C_{0,n}^1,\cdots,C_{m,n}^1,\cdots,C_{M,N}^1,C_{-2,0}^2,\cdots,C_{-2,n}^2,\cdots, \\ C_{-2,N}^2,\cdots,C_{-1,N}^2,C_{0,-2}^3,C_{0,-1}^3,\cdots,C_{m,-2}^3,\cdots,C_{M,-1}^3 \end{array} \right\}^T \quad (27)$$

$$\mathbf{D}_{mn} = \left\{ \begin{array}{l} D_{0,0}^1,\cdots,D_{0,n}^1,\cdots,D_{m,n}^1,\cdots,D_{M,N}^1,D_{-2,0}^2,\cdots,D_{-2,n}^2,\cdots, \\ D_{-2,N}^2,\cdots,D_{-1,N}^2,D_{0,-2}^3,D_{0,-1}^3,\cdots,D_{m,-2}^3,\cdots,D_{M,-1}^3 \end{array} \right\}^T \quad (28)$$

$$\mathbf{E}_{mn} = \left\{ \begin{array}{l} E_{0,0}^1,\cdots,E_{0,n}^1,\cdots,E_{m,n}^1,\cdots,E_{M,N}^1,E_{-2,0}^2,\cdots,E_{-2,n}^2,\cdots, \\ E_{-2,N}^2,\cdots,E_{-1,N}^2,E_{0,-2}^3,E_{0,-1}^3,\cdots,E_{m,-2}^3,\cdots,E_{M,-1}^3 \end{array} \right\}^T \quad (29)$$

$$\mathbf{F}_{m_t n_t l_t} = \left\{ \begin{array}{l} F_{0,0,0}^1,\cdots,F_{0,0,l_t}^1,\cdots,F_{0,0,L_t}^1,\cdots,F_{0,N_t,L_t}^1,\cdots,F_{m_t,n_t,l_t}^1,\cdots,F_{M_t,N_t,L_t}^1, \\ F_{-2,0,0}^2,\cdots,F_{-2,0,l_t}^2,\cdots,F_{-2,0,L_t}^2,\cdots,F_{-2,n_t,l_t}^2,\cdots,F_{-1,n_t,l_t}^2,\cdots,F_{-1,N_t,L_t}^2, \\ F_{0,-2,0}^3,\cdots,F_{0,-2,l_t}^3,\cdots,F_{0,-2,L_t}^3,\cdots,F_{m_t,-2,l_t}^3,\cdots,F_{m_t,-1,l_t}^3,\cdots,F_{M_t,-1,L_t}^3, \\ F_{0,0,-2}^4,F_{0,0,-1}^4,\cdots,F_{0,N_t,-2}^4,\cdots,F_{m_t,n_t,-2}^4,\cdots,F_{m_t,n_t,-1}^4,\cdots,F_{M_t,N_t,-1}^4, \\ F_{-2,-2,0}^5,\cdots,F_{-2,-2,l_t}^5,\cdots,F_{-2,-2,L_t}^5,\cdots,F_{-2,-1,l_t}^5,\cdots,F_{-2,-1,L_t}^5,\cdots,F_{-1,-1,L_t}^5, \\ F_{-2,0,-2}^6,F_{-2,0,-1}^6,\cdots,F_{-2,n_t,-2}^6,\cdots,F_{-2,N_t,-2}^6,\cdots,F_{-1,n_t,L_t}^6,\cdots,F_{-1,N_t,-1}^6, \\ F_{0,-2,-2}^7,F_{0,-2,-1}^7,\cdots,F_{m_t,-2,-2}^7,\cdots,F_{m_t,-1,-1}^7,\cdots,F_{M_t,-2,-2}^7,\cdots,F_{M_t,-1,-1}^7 \end{array} \right\}^T \quad (30)$$

$$
\mathbf{G}_{m_t n_t l_t} = \left\{
\begin{array}{l}
G^1_{0,0,0}, \cdots, G^1_{0,0,l_t}, \cdots, G^1_{0,0,L_t}, \cdots, G^1_{0,N_t,L_t}, \cdots, G^1_{m_t,n_t,l_t}, \cdots, G^1_{M_t,N_t,L_t}, \\
G^2_{-2,0,0}, \cdots, G^2_{-2,0,l_t}, \cdots, G^2_{-2,0,L_t}, \cdots, G^2_{-2,n_t,l_t}, \cdots, G^2_{-1,n_t,l_t}, \cdots, G^2_{-1,N_t,L_t}, \\
G^3_{0,-2,0}, \cdots, G^3_{0,-2,l_t}, \cdots, G^3_{0,-2,L_t}, \cdots, G^3_{m_t,-2,l_t}, \cdots, G^3_{m_t,-1,l_t}, \cdots, G^3_{M_t,-1,L_t}, \\
G^4_{0,0,-2}, G^4_{0,0,-1}, \cdots, G^4_{0,N_t,-2}, \cdots, G^4_{m_t,n_t,-2}, \cdots, G^4_{m_t,n_t,-1}, \cdots, G^4_{M_t,N_t,-1}, \\
G^5_{-2,-2,0}, \cdots, G^5_{-2,-2,l_t}, \cdots, G^5_{-2,-2,L_t}, \cdots, G^5_{-2,-1,l_t}, \cdots, G^5_{-2,-1,L_t}, \cdots, G^5_{-1,-1,L_t}, \\
G^6_{-2,0,-2}, G^6_{-2,0,-1}, \cdots, G^6_{-2,n_t,-2}, \cdots, G^6_{-2,N_t,-2}, \cdots, G^6_{-1,n_t,L_t}, \cdots, G^6_{-1,N_t,-1}, \\
G^7_{0,-2,-2}, G^7_{0,-2,-1}, \cdots, G^7_{m_t,-2,-2}, \cdots, G^7_{m_t,-1,-1}, \cdots, G^7_{M_t,-2,-2}, \cdots, G^7_{M_t,-1,-1}
\end{array}
\right\}^T
$$
(31)

where $\lambda^\alpha_m = m\pi/\alpha$, $\lambda^\beta_n = n\pi/\beta$, $\lambda^{\alpha_n}_{m_t} = m_t\pi/\alpha_n$, $\lambda^{\alpha_n}_{n_t} = n_t\pi/\alpha_n$, $\lambda^{\alpha_n}_{l_t} = l_t\pi/\alpha_n$ ($n = 1, 2$).

2.4 Stress–strain and displacement relationship

The normal strain and shear strain at any point on the composite laminated plate can be defined by the changes of strain and curvature in midplane:

$$
\left\{
\begin{array}{l}
\varepsilon_r = \varepsilon^0_r + z\chi_r \\
\varepsilon_\theta = \varepsilon^0_\theta + z\chi_\theta
\end{array}
\right.
\quad
\left\{
\begin{array}{l}
\gamma_{r\theta} = \gamma^0_{r\theta} + z\chi_{r\theta} \\
\gamma_{rz} = \gamma^0_{rz} \\
\gamma_{\theta z} = \gamma^0_{\theta z}
\end{array}
\right.
$$
(32)

where ε^0_r, ε^0_θ, $\gamma^0_{r\theta}$, γ^0_{rz} and $\gamma^0_{\theta z}$ are the strain components on the middle surface of the laminated plate, and χ_r, χ_θ and $\chi_{r\theta}$ are the curvature variation components on the middle surface. The specific expressions are as follows:

$$
\varepsilon^0_r = \frac{\partial u}{\partial r} \quad \varepsilon^0_\theta = \frac{\partial v}{r\partial\theta} + \frac{u}{r}
$$

$$
\gamma^0_{r\theta} = \frac{\partial v}{\partial r} + \frac{\partial u}{r\partial\theta} - \frac{v}{r} \quad \gamma^0_{rz} = \frac{\partial w}{\partial r} + \phi_r \quad \gamma^0_{\theta z} = \phi_\theta
$$
(33)

$$
\chi_r = \frac{\partial \phi_r}{\partial r} \quad \chi_\theta = \frac{\partial \phi_\theta}{r\partial\theta} + \frac{\phi_r}{r} \quad \chi_{r\theta} = \frac{\partial \phi_\theta}{\partial r} + \frac{\partial \phi_r}{r\partial\theta} - \frac{\phi_\theta}{r}
$$

According to Hooke's law, the corresponding stress–strain relationship at the k-layer can be obtained as follows:

$$
\left\{
\begin{array}{c}
\sigma_r \\
\sigma_\theta \\
\tau_{r\theta} \\
\tau_{rz} \\
\tau_{\theta z}
\end{array}
\right\}
=
\begin{bmatrix}
\overline{Q^k_{11}} & \overline{Q^k_{12}} & & & \overline{Q^k_{16}} \\
\overline{Q^k_{21}} & \overline{Q^k_{22}} & & & \overline{Q^k_{26}} \\
& & \overline{Q^k_{44}} & \overline{Q^k_{45}} & \\
& & \overline{Q^k_{54}} & \overline{Q^k_{55}} & \\
\overline{Q^k_{61}} & \overline{Q^k_{62}} & & & \overline{Q^k_{66}}
\end{bmatrix}
\left\{
\begin{array}{c}
\varepsilon_r \\
\varepsilon_\theta \\
\gamma_{r\theta} \\
\gamma_{rz} \\
\gamma_{\theta z}
\end{array}
\right\}
$$
(34)

where the stiffness coefficients of laminated plate can be denoted by $\overline{Q^k_{ij}}$ ($i, j = 1, 2, \ldots, 6$), and they can be acquired from the following equations:

$$
\begin{bmatrix}
\overline{Q^k_{11}} & \overline{Q^k_{12}} & & & & \overline{Q^k_{16}} \\
\overline{Q^k_{21}} & \overline{Q^k_{22}} & & & & \overline{Q^k_{26}} \\
& & \overline{Q^k_{44}} & \overline{Q^k_{45}} & & \\
& & \overline{Q^k_{54}} & \overline{Q^k_{55}} & & \\
\overline{Q^k_{61}} & \overline{Q^k_{62}} & & & & \overline{Q^k_{66}}
\end{bmatrix}
= \mathbf{T}
\begin{bmatrix}
Q^k_{11} & Q^k_{12} & & & \\
Q^k_{21} & Q^k_{22} & & & \\
& & Q^k_{44} & & \\
& & & Q^k_{55} & \\
& & & & Q^k_{66}
\end{bmatrix}
\mathbf{T}^T
\tag{35}
$$

In Equation (35), $\mathbf{T}$ is the transformation matrix, which is defined as follows, where θ is the included angle between the main direction and the r direction of the layer, namely, the layer laying direction:

$$
\mathbf{T} =
\begin{bmatrix}
\cos^2\theta & \sin^2\theta & & & -2\sin\theta\cos\theta \\
\sin^2\theta & \cos^2\theta & & & 2\sin\theta\cos\theta \\
& & \cos\theta & \sin\theta & \\
& & -\sin\theta & \cos\theta & \\
\sin\theta\cos\theta & -\sin\theta\cos\theta & & & \cos^2\theta - \sin^2\theta
\end{bmatrix}
\tag{36}
$$

in which Q^k_{ij} $(i, j = 1, 2, \ldots, 6)$ denotes the material coefficient of the k-layer of plate, and its value can be obtained by the engineering constant:

$$
Q^k_{11} = \frac{E_1}{1 - \mu_{12}\mu_{21}} \quad Q^k_{12} = \frac{\mu_{12}E_2}{1 - \mu_{12}\mu_{21}} = Q^k_{21} \quad Q^k_{22} = \frac{E_2}{1 - \mu_{12}\mu_{21}}
$$

$$
Q^k_{44} = G_{23} \quad Q^k_{55} = G_{13} \quad Q^k_{66} = G_{12}
\tag{37}
$$

The forces and torques applied to the laminated plate are obtained by integrating the stresses in the plane. From one layer of laminated plate to another layer, the thickness is integrated to obtain the following equation:

$$
\begin{bmatrix}
N_r \\ N_\theta \\ N_{r\theta} \\ M_r \\ M_\theta \\ M_{r\theta}
\end{bmatrix}
=
\begin{bmatrix}
A_{11} & A_{12} & A_{16} & B_{11} & B_{12} & B_{16} \\
A_{12} & A_{22} & A_{26} & B_{12} & B_{22} & B_{26} \\
A_{16} & A_{26} & A_{66} & B_{16} & B_{26} & B_{66} \\
B_{11} & B_{12} & B_{16} & D_{11} & D_{12} & D_{16} \\
B_{12} & B_{22} & B_{26} & D_{12} & D_{22} & D_{26} \\
B_{16} & B_{26} & B_{66} & D_{16} & D_{26} & D_{66}
\end{bmatrix}
\begin{bmatrix}
\varepsilon^0_r \\ \varepsilon^0_\theta \\ \gamma^0_{r\theta} \\ \chi_r \\ \chi_\theta \\ \chi_{r\theta}
\end{bmatrix}
\tag{38}
$$

$$
\begin{bmatrix}
Q_\theta \\ Q_r
\end{bmatrix}
= \overline{\kappa_s}
\begin{bmatrix}
A_{44} & A_{45} \\
A_{45} & A_{55}
\end{bmatrix}
\begin{bmatrix}
\gamma^0_{\theta z} \\ \gamma^0_{rz}
\end{bmatrix}
\tag{39}
$$

$$
A_{ij} = \sum_{k=1}^{N_L} \overline{Q^k_{ij}}(Z_{k+1} - Z_k) \quad B_{ij} = \frac{1}{2}\sum_{k=1}^{N_L} \overline{Q^k_{ij}}(Z^2_{k+1} - Z^2_k) \quad D_{ij} = \frac{1}{3}\sum_{k=1}^{N_L} \overline{Q^k_{ij}}(Z^3_{k+1} - Z^3_k) \tag{40}
$$

where N_r, N_θ and $N_{r\theta}$ are the resultant forces in the plane, M_r, M_θ and $M_{r\theta}$ represent bending and torsional torque and Q_θ, Q_r denote the resultant forces of horizontal shear. Shear correction factor which can guarantee the strain energy caused by transverse shear stress is expressed as $\overline{\kappa_s}$, and N_L represents the number of layers.

2.5 Energy equation and solution procedure

The Lagrange equation of *t* the conical–cylindrical acoustic cavity coupled system and rotary composite laminated plate and conical–cylindrical double cavities coupled system can be expressed as follows:

$$L_P = T_P - U_P - U_{P-coupling} - U_{SP} - W_{P\&C_1} - W_{P\&C_2} + W_F \tag{41}$$

$$L_{C_1} = T_{C_1} - U_{C_1} - U_{C_1-coupling} - W_{C_1\&P} - W_{C_1\&C_2} + W_{C_1-wall} + W_{Q_1} \tag{42}$$

$$L_{C_2} = T_{C_2} - U_{C_2} - U_{C_2-coupling} - W_{C_2\&P} - W_{C_2\&C_1} + W_{C_2-wall} + W_{Q_2} \tag{43}$$

where T_P and T_{C_n} ($n = 1, 2$) are the total kinetic energy of the rotary composite plate and the nth acoustic cavity in the coupled systems, respectively. U_P and U_{C_n} separately denote the total potential energy in the plate and the nth acoustic cavity. $U_{P-coupling}$ and $U_{C_n-coupling}$ represent the coupling potential energy of the composite laminated plate and acoustic cavities when rotation angle $\vartheta = 2\pi$. The boundary spring potential energy of plate can be expressed as U_{SP}. $W_{P\&C_1}$, $W_{P\&C_2}$, $W_{C_1\&P}$ and $W_{C_2\&P}$ are the coupling potential energy generated when the composite plate is coupled with acoustic cavity 1 and acoustic cavity 2, and $W_{P\&C_1} = W_{C_1\&P}$, $W_{P\&C_2} = W_{C_2\&P}$. W_{C_n-wall} represents the impedance potential energy caused by the impedance wall of the nth acoustic cavity in the coupled systems. $W_{C_1\&C_2}$ and $W_{C_2\&C_1}$ denote the coupling potential energy between acoustic cavity 1 and acoustic cavity 2, in which $W_{C_1\&C_2} = W_{C_2\&C_1}$. W_F is the work done by harmonic point force F on the composite laminated plate, and W_{Q_n} is the work done by the monopole point sound source in the nth acoustic cavity of the coupled systems.

For the two coupled systems, partial energy equations do not exist completely: (1) the conical–cylindrical acoustic cavity coupled system: $L_P = 0$, $W_{P\&C_1} = W_{C_1\&P} = 0$, $W_{P\&C_2} = W_{C_2\&P} = 0$; (2) the rotary composite laminated plate and conical–cylindrical double cavities coupled system: $W_{C_1\&C_2} = W_{C_2\&C_1} = 0$.

The total kinetic energy of the rotating composite laminated plate and the nth acoustic cavity represented by T_P and T_{C_n} can be written as follows:

$$T_P = \frac{1}{2}\omega^2 \int_0^H \int_0^\vartheta \left\{ \begin{array}{l} I_0\left[\mathbf{A}_{mn}^2 + \mathbf{B}_{mn}^2 + \mathbf{C}_{mn}^2\right]\left(\Phi^M + \sum_{N_q=1}^2 \Phi^{N_q}\right)^2 + \\[2ex] 2I_1[\mathbf{A}_{mn}\mathbf{D}_{mn} + \mathbf{B}_{mn}\mathbf{E}_{mn}]\left(\Phi^M + \sum_{N_q=1}^2 \Phi^{N_q}\right)^2 + \\[2ex] I_2\left[\mathbf{D}_{mn}^2 + \mathbf{E}_{mn}^2\right]\left(\Phi^M + \sum_{N_q=1}^2 \Phi^{N_q}\right)^2 \end{array} \right\} (r + R_2)drd\theta \tag{44}$$

$$I_0 = \sum_{k=1}^{N_l} \int_{Z_k}^{Z_{k+1}} \rho^k dz \quad I_1 = \sum_{k=1}^{N_l} \int_{Z_k}^{Z_{k+1}} \rho^k \cdot z dz \quad I_2 = \sum_{k=1}^{N_l} \int_{Z_k}^{Z_{k+1}} \rho^k \cdot z^2 dz \tag{45}$$

$$T_{C_1} = \frac{1}{2\rho_{C_1}\omega^2} \int_0^{L_{\alpha_1}} \int_0^{L_{\beta_1}} \int_0^{L_{z_1}} \left\{ \begin{array}{l} \left(\left[(J_{11}^1)^2 + (J_{21}^1)^2 \right] \left(\frac{\partial \mathbf{P}_1^{\Omega}}{H_{z_1}\partial z_1} + \sum_{\Theta_q=1}^{6} \frac{\partial \mathbf{P}_1^{\Theta_q}}{H_{z_1}\partial z_1} \right) \right)^2 + \\[2ex] (J_{11}^1 \cdot J_{21}^1) \left(\frac{\partial \mathbf{P}_1^{\Omega}}{H_{z_1}\partial z_1} + \sum_{\Theta_q=1}^{6} \frac{\partial \mathbf{P}_1^{\Theta_q}}{H_{z_1}\partial z_1} \right) \left(\frac{\partial \mathbf{P}_1^{\Omega}}{H_{\alpha_1}\partial \alpha_1} + \sum_{\Theta_q=1}^{6} \frac{\partial \mathbf{P}_1^{\Theta_q}}{H_{\alpha_1}\partial \alpha_1} \right) + \\[2ex] \left(\left[(J_{12}^1)^2 + (J_{22}^1)^2 \right] \left(\frac{\partial \mathbf{P}_1^{\Omega}}{H_{\alpha_1}\partial \alpha_1} + \sum_{\Theta_q=1}^{6} \frac{\partial \mathbf{P}_1^{\Theta_q}}{H_{\alpha_1}\partial \alpha_1} \right) \right)^2 + \\[2ex] (J_{12}^1 \cdot J_{22}^1) \left(\frac{\partial \mathbf{P}_1^{\Omega}}{H_{z_1}\partial z_1} + \sum_{\Theta_q=1}^{6} \frac{\partial \mathbf{P}_1^{\Theta_q}}{H_{z_1}\partial z_1} \right) \left(\frac{\partial \mathbf{P}_1^{\Omega}}{H_{\alpha_1}\partial \alpha_1} + \sum_{\Theta_q=1}^{6} \frac{\partial \mathbf{P}_1^{\Theta_q}}{H_{\alpha_1}\partial \alpha_1} \right) + \\[2ex] \left[\frac{\partial \mathbf{P}_1^{\Omega}}{H_{\beta_1}\partial \beta_1} + \sum_{\Theta_q=1}^{6} \frac{\partial \mathbf{P}_1^{\Theta_q}}{H_{\beta_1}\partial \beta_1} \right]^2 \end{array} \right\}$$

$$\mathbf{F}_{m_t n_t l_t} \cdot |J_1| \cdot H_{\alpha_1} H_{\beta_1} H_{z_1} d\alpha_1 d\beta_1 dz_1$$

(46)

$$T_{C_2} = \frac{1}{2\rho_{C_2}\omega^2} \int_0^{L_{\alpha_2}} \int_0^{L_{\beta_2}} \int_0^{L_{z_2}} \left\{ \begin{array}{l} \left(\left[(J_{11}^2)^2 + (J_{21}^2)^2 \right] \left(\frac{\partial \mathbf{P}_2^{\Omega}}{H_{z_2}\partial z_2} + \sum_{\Theta_q=1}^{6} \frac{\partial \mathbf{P}_2^{\Theta_q}}{H_{z_2}\partial z_2} \right) \right)^2 + \\[2ex] (J_{11}^2 \cdot J_{21}^2) \left(\frac{\partial \mathbf{P}_2^{\Omega}}{H_{z_2}\partial z_2} + \sum_{\Theta_q=1}^{6} \frac{\partial \mathbf{P}_2^{\Theta_q}}{H_{z_2}\partial z_2} \right) \left(\frac{\partial \mathbf{P}_2^{\Omega}}{H_{\alpha_2}\partial \alpha_2} + \sum_{\Theta_q=1}^{6} \frac{\partial \mathbf{P}_2^{\Theta_q}}{H_{\alpha_2}\partial \alpha_2} \right) + \\[2ex] \left(\left[(J_{12}^2)^2 + (J_{22}^2)^2 \right] \left(\frac{\partial \mathbf{P}_2^{\Omega}}{H_{\alpha_2}\partial \alpha_2} + \sum_{\Theta_q=1}^{6} \frac{\partial \mathbf{P}_2^{\Theta_q}}{H_{\alpha_2}\partial \alpha_2} \right) \right)^2 + \\[2ex] (J_{12}^2 \cdot J_{22}^2) \left(\frac{\partial \mathbf{P}_2^{\Omega}}{H_{z_2}\partial z_2} + \sum_{\Theta_q=1}^{6} \frac{\partial \mathbf{P}_2^{\Theta_q}}{H_{z_2}\partial z_2} \right) \left(\frac{\partial \mathbf{P}_2^{\Omega}}{H_{\alpha_2}\partial \alpha_2} + \sum_{\Theta_q=1}^{6} \frac{\partial \mathbf{P}_2^{\Theta_q}}{H_{\alpha_2}\partial \alpha_2} \right) + \\[2ex] \left[\frac{\partial \mathbf{P}_2^{\Omega}}{H_{\beta_2}\partial \beta_2} + \sum_{\Theta_q=1}^{6} \frac{\partial \mathbf{P}_2^{\Theta_q}}{H_{\beta_2}\partial \beta_2} \right]^2 \end{array} \right\}$$

$$\mathbf{G}_{m_t n_t l_t} \cdot |J_2| \cdot H_{\alpha_2} H_{\beta_2} H_{z_2} d\alpha_2 d\beta_2 dz_2$$

(47)

in which N_l represents the number of layers of rotary composite laminated plate. Z_k is the coordinate value of bottom surface thickness of k-layer, and Z_{k+1} is the coordinate value of upper surface thickness. The material density of k-layer can be expressed as ρ^k, and ρ_{C_n} denotes the density of acoustic media in nth acoustic cavity.

The specific expressions of the total potential energy U_P and U_{C_n} are as follows:

$$U_P = U_{\text{stretch}} + U_{\text{bend}} + U_{\text{s-b}} = \frac{1}{2}\int_0^H \int_0^\vartheta \left\{ \begin{array}{l} N_r\varepsilon_r^0 + N_r\varepsilon_r^0 + N_{r\theta}\gamma_{r\theta}^0 + M_r\chi_r + \\ M_\theta\chi_\theta + M_{r\theta}\chi_{r\theta} + Q_r\gamma_{rz}^0 + Q_\theta\gamma_{\theta z}^0 \end{array} \right\} r\,dr\,d\theta \quad (48)$$

$$U_{\text{stretch}} = \frac{1}{2}\int_0^H \int_0^\vartheta$$

$$
\left\{
\begin{array}{l}
\left(\overline{\kappa_s}A_{44}\mathbf{E}_{mn}^2 + 2\overline{\kappa_s}A_{45}\mathbf{D}_{mn}\mathbf{E}_{mn} + \overline{\kappa_s}A_{55}\mathbf{D}_{mn}^2\right)\left(\Phi^M + \displaystyle\sum_{N_q=1}^2 \Phi^{N_q}\right)^2 + \\[4mm]
\left(A_{11}\mathbf{A}_{mn}^2 + 2A_{16}\mathbf{A}_{mn}\mathbf{B}_{mn} + A_{66}\mathbf{B}_{mn}^2 + \overline{\kappa_s}A_{55}\mathbf{C}_{mn}^2\right)\left(\dfrac{\partial\Phi^M}{\partial r} + \displaystyle\sum_{N_q=1}^2 \dfrac{\partial\Phi^{N_q}}{\partial r}\right)^2 + \\[4mm]
+\left(A_{22}\mathbf{A}_{mn}^2 - 2A_{26}\mathbf{A}_{mn}\mathbf{B}_{mn} + A_{66}\mathbf{B}_{mn}^2\right)\left(\dfrac{\Phi^M}{(r+R_2)} + \displaystyle\sum_{N_q=1}^2 \dfrac{\Phi^{N_q}}{(r+R_2)}\right)^2 + \\[4mm]
\left(\begin{array}{l}A_{22}\mathbf{B}_{mn}^2 + 2A_{26}\mathbf{A}_{mn}\mathbf{B}_{mn} + A_{66}\mathbf{A}_{mn}^2 \\ +\overline{\kappa_s}A_{44}\mathbf{C}_{mn}^2\end{array}\right)\left(\dfrac{\partial\Phi^M}{(r+R_2)\partial\theta} + \displaystyle\sum_{N_q=1}^2 \dfrac{\partial\Phi^{N_q}}{(r+R_2)\partial\theta}\right)^2 + \\[4mm]
\left(\begin{array}{l}2A_{12}\mathbf{A}_{mn}^2 - 2A_{16}\mathbf{A}_{mn}\mathbf{B}_{mn} \\ +2A_{26}\mathbf{A}_{mn}\mathbf{B}_{mn} - 2A_{66}\mathbf{B}_{mn}^2\end{array}\right)\left(\dfrac{\Phi^M}{(r+R_2)} + \displaystyle\sum_{N_q=1}^2 \dfrac{\Phi^{N_q}}{(r+R_2)}\right)\left(\dfrac{\partial\Phi^M}{\partial r} + \displaystyle\sum_{N_q=1}^2 \dfrac{\partial\Phi^{N_q}}{\partial r}\right) + \\[4mm]
\left(\begin{array}{l}2A_{12}\mathbf{A}_{mn}\mathbf{B}_{mn} + 2A_{16}\mathbf{A}_{mn}^2 + 2A_{26}\mathbf{B}_{mn}^2 \\ +2A_{66}\mathbf{A}_{mn}\mathbf{B}_{mn} + 2\overline{\kappa_s}A_{45}\mathbf{C}_{mn}^2\end{array}\right)\left(\dfrac{\partial\Phi^M}{(r+R_2)\partial\theta} + \displaystyle\sum_{N_q=1}^2 \dfrac{\partial\Phi^{N_q}}{(r+R_2)\partial\theta}\right)\left(\dfrac{\partial\Phi^M}{\partial r} + \displaystyle\sum_{N_q=1}^2 \dfrac{\partial\Phi^{N_q}}{\partial r}\right) \\[4mm]
+\left(\begin{array}{l}2A_{22}\mathbf{A}_{mn}\mathbf{B}_{mn} + 2A_{26}\mathbf{A}_{mn}^2 \\ -2A_{66}\mathbf{A}_{mn}\mathbf{B}_{mn} - 2A_{26}\mathbf{B}_{mn}^2\end{array}\right)\left(\dfrac{\Phi^M}{(r+R_2)} + \displaystyle\sum_{N_q=1}^2 \dfrac{\Phi^{N_q}}{(r+R_2)}\right)\left(\dfrac{\partial\Phi^M}{(r+R_2)\partial\theta} + \displaystyle\sum_{N_q=1}^2 \dfrac{\partial\Phi^{N_q}}{(r+R_2)\partial\theta}\right) \\[4mm]
+\left(2\overline{\kappa_s}A_{44}\mathbf{C}_{mn}\mathbf{E}_{mn} + 2\overline{\kappa_s}A_{45}\mathbf{C}_{mn}\mathbf{D}_{mn}\right)\left(\Phi^M + \displaystyle\sum_{N_q=1}^2 \Phi^{N_q}\right)\left(\dfrac{\partial\Phi^M}{(r+R_2)\partial\theta} + \displaystyle\sum_{N_q=1}^2 \dfrac{\partial\Phi^{N_q}}{(r+R_2)\partial\theta}\right) \\[4mm]
+\left(2\overline{\kappa_s}A_{44}\mathbf{C}_{mn}\mathbf{E}_{mn} + 2\overline{\kappa_s}A_{45}\mathbf{C}_{mn}\mathbf{D}_{mn}\right)\left(\Phi^M + \displaystyle\sum_{N_q=1}^2 \Phi^{N_q}\right)\left(\dfrac{\partial\Phi^M}{\partial r} + \displaystyle\sum_{N_q=1}^2 \dfrac{\partial\Phi^{N_q}}{\partial r}\right)
\end{array}
\right\}
$$

$$(r+R_2)dr\,d\theta$$

$$(49)$$

$$U_{\text{bend}} = \frac{1}{2} \int_0^H \int_0^\vartheta \left\{ \begin{array}{l} \left(D_{11}\mathbf{D}_{mn}^2 + 2D_{16}\mathbf{D}_{mn}\mathbf{E}_{mn} + D_{66}\mathbf{E}_{mn}^2\right)\left(\dfrac{\partial\Phi^M}{\partial r} + \sum\limits_{N_q=1}^2 \dfrac{\partial\Phi^{N_q}}{\partial r}\right)^2 + \\[3mm] \left(D_{22}\mathbf{E}_{mn}^2 + D_{66}\mathbf{D}_{mn}^2 + 2D_{26}\mathbf{D}_{mn}\mathbf{E}_{mn}\right)\left(\dfrac{\partial\Phi^M}{(r+R_2)\partial\theta} + \sum\limits_{N_q=1}^2 \dfrac{\partial\Phi^{N_q}}{(r+R_2)\partial\theta}\right)^2 + \\[3mm] \left(D_{22}\mathbf{D}_{mn}^2 + D_{66}\mathbf{E}_{mn}^2 - 2D_{26}\mathbf{D}_{mn}\mathbf{E}_{mn}\right)\left(\dfrac{\Phi^M}{(r+R_2)} + \sum\limits_{N_q=1}^2 \dfrac{\Phi^{N_q}}{(r+R_2)}\right)^2 + \\[3mm] \left(\begin{array}{c} 2D_{12}\mathbf{D}_{mn}\mathbf{E}_{mn} + 2D_{16}\mathbf{D}_{mn}^2 \\ + 2D_{66}\mathbf{D}_{mn}\mathbf{E}_{mn} + 2D_{26}\mathbf{E}_{mn}^2 \end{array}\right)\left(\dfrac{\partial\Phi^M}{\partial r} + \sum\limits_{N_q=1}^2 \dfrac{\partial\Phi^{N_q}}{\partial r}\right)\left(\dfrac{\partial\Phi^M}{(r+R_2)\partial\theta} + \sum\limits_{N_q=1}^2 \dfrac{\partial\Phi^{N_q}}{(r+R_2)\partial\theta}\right) + \\[3mm] \left(\begin{array}{c} 2D_{12}\mathbf{D}_{mn}^2 - 2D_{16}\mathbf{D}_{mn}\mathbf{E}_{mn} \\ - 2D_{66}\mathbf{E}_{mn}^2 + 2D_{26}\mathbf{D}_{mn}\mathbf{E}_{mn} \end{array}\right)\left(\dfrac{\partial\Phi^M}{\partial r} + \sum\limits_{N_q=1}^2 \dfrac{\partial\Phi^{N_q}}{\partial r}\right)\left(\dfrac{\Phi^M}{(r+R_2)} + \sum\limits_{N_q=1}^2 \dfrac{\Phi^{N_q}}{(r+R_2)}\right) + \\[3mm] \left(\begin{array}{c} 2D_{22}\mathbf{D}_{mn}\mathbf{E}_{mn} - 2D_{26}\mathbf{E}_{mn}^2 \\ - 2D_{66}\mathbf{D}_{mn}\mathbf{E}_{mn} + 2D_{26}\mathbf{D}_{mn}^2 \end{array}\right)\left(\dfrac{\partial\Phi^M}{(r+R_2)\partial\theta} + \sum\limits_{N_q=1}^2 \dfrac{\partial\Phi^{N_q}}{(r+R_2)\partial\theta}\right)\left(\dfrac{\Phi^M}{(r+R_2)} + \sum\limits_{N_q=1}^2 \dfrac{\Phi^{N_q}}{(r+R_2)}\right) \end{array} \right\}$$

$$(r+R_2)drd\theta$$

$$(50)$$

$$U_{\text{s-b}} = \int_0^H \int_0^\vartheta \left\{ \begin{array}{l} \left[\begin{array}{c} B_{11}\mathbf{A}_{mn}\mathbf{D}_{mn} + B_{16}(\mathbf{A}_{mn}\mathbf{E}_{mn} + \mathbf{B}_{mn}\mathbf{D}_{mn}) \\ + B_{66}\mathbf{B}_{mn}\mathbf{E}_{mn} \end{array}\right]\left(\dfrac{\partial\Phi^M}{\partial r} + \sum\limits_{N_q=1}^2 \dfrac{\partial\Phi^{N_q}}{\partial r}\right)^2 + \\[3mm] \left[\begin{array}{c} B_{22}\mathbf{B}_{mn}\mathbf{E}_{mn} + B_{26}(\mathbf{A}_{mn}\mathbf{E}_{mn} + \mathbf{B}_{mn}\mathbf{D}_{mn}) \\ + B_{66}\mathbf{A}_{mn}\mathbf{D}_{mn} \end{array}\right]\left(\dfrac{\partial\Phi^M}{(r+R_2)\partial\theta} + \sum\limits_{N_q=1}^2 \dfrac{\partial\Phi^{N_q}}{(r+R_2)\partial\theta}\right)^2 + \\[3mm] \left[\begin{array}{c} B_{22}\mathbf{A}_{mn}\mathbf{D}_{mn} - B_{26}(\mathbf{A}_{mn}\mathbf{E}_{mn} + \mathbf{B}_{mn}\mathbf{D}_{mn}) \\ + B_{66}\mathbf{B}_{mn}\mathbf{E}_{mn} \end{array}\right]\left(\dfrac{\Phi^M}{(r+R_2)} + \sum\limits_{N_q=1}^2 \dfrac{\Phi^{N_q}}{(r+R_2)}\right)^2 + \\[3mm] \left[\begin{array}{c} B_{12}(\mathbf{A}_{mn}\mathbf{E}_{mn} + \mathbf{B}_{mn}\mathbf{D}_{mn}) \\ + 2B_{16}\mathbf{A}_{mn}\mathbf{D}_{mn} + 2B_{26}\mathbf{B}_{mn}\mathbf{E}_{mn} \\ + B_{66}(\mathbf{A}_{mn}\mathbf{E}_{mn} + \mathbf{B}_{mn}\mathbf{D}_{mn}) \end{array}\right]\left(\dfrac{\partial\Phi^M}{\partial r} + \sum\limits_{N_q=1}^2 \dfrac{\partial\Phi^{N_q}}{\partial r}\right)\left(\dfrac{\partial\Phi^M}{(r+R_2)\partial\theta} + \sum\limits_{N_q=1}^2 \dfrac{\partial\Phi^{N_q}}{(r+R_2)\partial\theta}\right) + \\[3mm] \left[\begin{array}{c} 2B_{12}\mathbf{A}_{mn}\mathbf{D}_{mn} - 2B_{16}\mathbf{B}_{mn}\mathbf{E}_{mn} \\ - B_{16}(\mathbf{A}_{mn}\mathbf{E}_{mn} + \mathbf{B}_{mn}\mathbf{D}_{mn}) \\ + B_{26}(\mathbf{A}_{mn}\mathbf{E}_{mn} + \mathbf{B}_{mn}\mathbf{D}_{mn}) \end{array}\right]\left(\dfrac{\partial\Phi^M}{\partial r} + \sum\limits_{N_q=1}^2 \dfrac{\partial\Phi^{N_q}}{\partial r}\right)\left(\dfrac{\Phi^M}{(r+R_2)} + \sum\limits_{N_q=1}^2 \dfrac{\Phi^{N_q}}{(r+R_2)}\right) + \\[3mm] \left[\begin{array}{c} B_{22}(\mathbf{A}_{mn}\mathbf{E}_{mn} + \mathbf{B}_{mn}\mathbf{D}_{mn}) \\ + 2B_{26}(\mathbf{A}_{mn}\mathbf{D}_{mn} - \mathbf{B}_{mn}\mathbf{E}_{mn}) \\ + B_{66}(\mathbf{A}_{mn}\mathbf{E}_{mn} + \mathbf{B}_{mn}\mathbf{D}_{mn}) \end{array}\right]\left(\dfrac{\partial\Phi^M}{(r+R_2)\partial\theta} + \sum\limits_{N_q=1}^2 \dfrac{\partial\Phi^{N_q}}{(r+R_2)\partial\theta}\right)\left(\dfrac{\Phi^M}{(r+R_2)} + \sum\limits_{N_q=1}^2 \dfrac{\Phi^{N_q}}{(r+R_2)}\right) \end{array} \right\}$$

$$(r+R_2)drd\theta$$

$$(51)$$

$$U_{C_1} = \frac{1}{2\rho_{C_1}c_1^2}\int_0^{L_{\alpha_1}}\int_0^{L_{\beta_1}}\int_0^{L_{z_1}}\left\{\left(\mathbf{P}_1^\Omega + \sum_{\Theta_q=1}^6 \mathbf{P}_1^{\Theta_q}\right)^2\right\}\mathbf{F}_{m_t n_l l_t}^2 \cdot |J_1| \cdot H_{\alpha_1}H_{\beta_1}H_{z_1} d\alpha_1 d\beta_1 dz_1 \quad (52)$$

$$U_{C_2} = \frac{1}{2\rho_{C_2}c_2^2}\int_0^{L_{\alpha_2}}\int_0^{L_{\beta_2}}\int_0^{L_{z_2}}\left\{\left(\mathbf{P}_2^\Omega + \sum_{\Theta_q=1}^6 \mathbf{P}_2^{\Theta_q}\right)^2\right\}\mathbf{G}_{m_t n_l l_t}^2 \cdot |J_2| \cdot H_{\alpha_2}H_{\beta_2}H_{z_2} d\alpha_2 d\beta_2 dz_2 \quad (53)$$

In the formula, the total potential energy of rotary composite laminated plate includes tensile potential energy U_{stretch}, bending potential energy U_{bend}, tensile and bending coupling potential energy $U_{\text{s}-\text{b}}$, whose expressions have also been given, and c_n is the propagation speed of sound in the acoustic medium of the nth cavity.

As the boundary conditions of the rotary composite laminated plate model established in this paper are determined by the boundary springs, the boundary spring potential energy U_{SP} will be generated, and the expressions are as follows:

$$U_{SP} = U_{SP}^\theta + U_{SP}^r \quad (54)$$

$$U_{SP}^\theta = \frac{1}{2}\int_0^\vartheta\int_{-h_p/2}^{h_p/2}\left\{\begin{array}{l}\left[\left(\begin{array}{c}k_{r0}^u\mathbf{A}_{mn}^2 + k_{r0}^v\mathbf{B}_{mn}^2 + k_{r0}^w\mathbf{C}_{mn}^2 \\ +K_{r0}^r\mathbf{D}_{mn}^2 + K_{r0}^\theta\mathbf{E}_{mn}^2\end{array}\right)\left(\Phi^M + \sum_{N_q=1}^2 \Phi^{N_q}\right)^2\right]_{r=0} \\ +\left[\left(\begin{array}{c}k_{r0}^u\mathbf{A}_{mn}^2 + k_{r0}^v\mathbf{B}_{mn}^2 + k_{r0}^w\mathbf{C}_{mn}^2 \\ +K_{r0}^r\mathbf{D}_{mn}^2 + K_{r0}^\theta\mathbf{E}_{mn}^2\end{array}\right)\left(\Phi^M + \sum_{N_q=1}^2 \Phi^{N_q}\right)^2\right]_{r=H}\end{array}\right\}dzd\theta$$

$$(55)$$

$$U_{SP}^r = \frac{1}{2}\int_0^H\int_{-h_p/2}^{h_p/2}\left\{\begin{array}{l}\left[\left(\begin{array}{c}k_{\theta0}^u\mathbf{A}_{mn}^2 + k_{\theta0}^v\mathbf{B}_{mn}^2 + k_{\theta0}^w\mathbf{C}_{mn}^2 \\ +K_{\theta0}^r\mathbf{D}_{mn}^2 + K_{\theta0}^\theta\mathbf{E}_{mn}^2\end{array}\right)\left(\Phi^M + \sum_{N_q=1}^2 \Phi^{N_q}\right)^2\right]_{\theta=0} \\ +\left[\left(\begin{array}{c}k_{\theta\vartheta}^u\mathbf{A}_{mn}^2 + k_{\theta\vartheta}^v\mathbf{B}_{mn}^2 + k_{\theta\vartheta}^w\mathbf{C}_{mn}^2 \\ +K_{\theta\vartheta}^r\mathbf{D}_{mn}^2 + K_{\theta\vartheta}^\theta\mathbf{E}_{mn}^2\end{array}\right)\left(\Phi^M + \sum_{N_q=1}^2 \Phi^{N_q}\right)^2\right]_{\theta=\vartheta}\end{array}\right\}dzdr$$

$$(56)$$

When $0 < \vartheta < 2\pi$, the impedance wall dissipation energy of the nth sound cavity in the coupled systems is as follows:

$$W_{C_1-\text{wall}} = -\frac{1}{2j\omega Z_r}\iint_{S_r}\sum_{i=1}^6\left(\mathbf{P}_1^\Omega + \sum_{\Theta_q=1}^6 \mathbf{P}_1^{\Theta_q}\right)^2\mathbf{F}_{m_t n_l l_t}^2 dS_r \quad (57)$$

$$W_{C_2-\text{wall}} = -\frac{1}{2j\omega Z_r}\iint_{S_r}\sum_{i=1}^6\left(\mathbf{P}_2^\Omega + \sum_{\Theta_q=1}^6 \mathbf{P}_2^{\Theta_q}\right)^2\mathbf{G}_{m_t n_l l_t}^2 dS_r \quad (58)$$

$$W_{C_n-\text{wall}} = W_{\text{wall}_1}^n + W_{\text{wall}_2}^n + W_{\text{wall}_3}^n + W_{\text{wall}_4}^n + W_{\text{wall}_5}^n + W_{\text{wall}_6}^n \quad (59)$$

where j represents a pure imaginary number. S_r denotes the area of the rth uncoupled acoustic wall, and the corresponding acoustic wall impedance value is expressed by Z_r.

When $\vartheta = 2\pi$, the coupling potential energy of the middle plate $U_{\text{P-coupling}}$ and the nth acoustic cavity of the coupled systems $U_{\text{C}_n\text{-coupling}}$ can be written as follows:

$$U_{\text{P-coupling}} =$$

$$\frac{1}{2} \int_0^H \int_{-h_p/2}^{h_p/2} \left\{ \left(k_{uc}\mathbf{A}_{mn}^2 + k_{vc}\mathbf{B}_{mn}^2 + k_{wc}\mathbf{C}_{mn}^2 + K_{rc}\mathbf{D}_{mn}^2 + K_{\theta c}\mathbf{E}_{mn}^2 \right) \left[\left. \left(\boldsymbol{\Phi}^M + \sum_{N_q=1}^{2} \boldsymbol{\Phi}^{N_q} \right) \right|_{\theta=0^\circ} - \left. \left(\boldsymbol{\Phi}^M + \sum_{N_q=1}^{2} \boldsymbol{\Phi}^{N_q} \right) \right|_{\theta=360^\circ} \right]^2 \right\} dz \, dr \qquad (60)$$

$$U_{\text{C}_1\text{-coupling}} = \frac{1}{\rho_{C_1}\omega^2} \int_0^{L_{\alpha_1}} \int_0^{L_{z_1}} \left\{ \left. \left(\frac{\partial \mathbf{P}_1^\Omega}{H_{\beta_1}\partial\beta_1} + \sum_{\Theta_q=1}^{6} \frac{\partial \mathbf{P}_1^{\Theta_q}}{H_{\beta_1}\partial\beta_1} \right) \right|_{\beta_1=0} * \left. \left(\mathbf{P}_1^\Omega + \sum_{\Theta_q=1}^{6} \mathbf{P}_1^{\Theta_q} \right) \right|_{\beta_1=0} - \left. \left(\frac{\partial \mathbf{P}_1^\Omega}{H_{\beta_1}\partial\beta_1} + \sum_{\Theta_q=1}^{6} \frac{\partial \mathbf{P}_1^{\Theta_q}}{H_{\beta_1}\partial\beta_1} \right) \right|_{\beta_1=2\pi} * \left. \left(\mathbf{P}_1^\Omega + \sum_{\Theta_q=1}^{6} \mathbf{P}_1^{\Theta_q} \right) \right|_{\beta_1=2\pi} \right\}$$

$$\mathbf{F}_{m_t n_t l_t}^2 \cdot |J_1| \cdot H_{\alpha_1} H_{z_1} d\alpha_1 \, dz_1$$

$$(61)$$

$$U_{\text{C}_2\text{-coupling}} = \frac{1}{\rho_{C_2}\omega^2} \int_0^{L_{\alpha_2}} \int_0^{L_{z_2}} \left\{ \left. \left(\frac{\partial \mathbf{P}_2^\Omega}{H_{\beta_2}\partial\beta_2} + \sum_{\Theta_q=1}^{6} \frac{\partial \mathbf{P}_2^{\Theta_q}}{H_{\beta_2}\partial\beta_2} \right) \right|_{\beta_2=0} * \left. \left(\mathbf{P}_2^\Omega + \sum_{\Theta_q=1}^{6} \mathbf{P}_2^{\Theta_q} \right) \right|_{\beta_2=0} - \left. \left(\frac{\partial \mathbf{P}_2^\Omega}{H_{\beta_2}\partial\beta_2} + \sum_{\Theta_q=1}^{6} \frac{\partial \mathbf{P}_2^{\Theta_q}}{H_{\beta_2}\partial\beta_2} \right) \right|_{\beta_2=2\pi} * \left. \left(\mathbf{P}_2^\Omega + \sum_{\Theta_q=1}^{6} \mathbf{P}_2^{\Theta_q} \right) \right|_{\beta_2=2\pi} \right\}$$

$$\mathbf{G}_{m_t n_t l_t}^2 \cdot |J_2| \cdot H_{\alpha_2} H_{z_2} d\alpha_2 \, dz_2$$

$$(62)$$

The coupling potential energy between acoustic cavity 1 and acoustic cavity 2 $W_{\text{C}_1\&\text{C}_2}$ can be expressed as follows:

$$W_{\text{C}_1\&\text{C}_2} =$$

$$\frac{1}{\rho_{C_2}\omega^2} \int_0^{L_{\alpha_1}} \int_0^{L_{\beta_1}} \left\{ \left. \left(\frac{\partial \mathbf{P}_2^\Omega}{H_{z_2}\partial z_2} + \sum_{\Theta_q=1}^{6} \frac{\partial \mathbf{P}_2^{\Theta_q}}{H_{z_2}\partial z_2} \right) \right|_{z_2=L_2} * \left. \left(\mathbf{P}_2^\Omega + \sum_{\Theta_q=1}^{6} \mathbf{P}_2^{\Theta_q} \right) \right|_{z_2=L_2} \mathbf{F}_{m_t n_t l_t}^2 - \left. \left(\frac{\partial \mathbf{P}_2^\Omega}{H_{z_2}\partial z_2} + \sum_{\Theta_q=1}^{6} \frac{\partial \mathbf{P}_2^{\Theta_q}}{H_{z_2}\partial z_2} \right) \right|_{z_2=L_2} * \left. \left(\mathbf{P}_1^\Omega + \sum_{\Theta_q=1}^{6} \mathbf{P}_1^{\Theta_q} \right) \right|_{z_1=0} \mathbf{F}_{m_t n_t l_t} \mathbf{G}_{m_t n_t l_t} \right\}$$

$$|J_2| \cdot H_{\alpha_2} H_{\beta_2} d\alpha_2 \, d\beta_2$$

$$(63)$$

$W_{\text{P}\&\text{C}_1}$ and $W_{\text{P}\&\text{C}_2}$ are the coupling potential energy when the laminated plate is coupled with acoustic cavity 1 and 2, respectively, and the expressions are as follows:

$$W_{P\&C_1} = \int_0^H \int_0^\vartheta \left\{ \begin{array}{l} \left(\Phi^M + \sum_{N_q=1}^2 \Phi^{N_q}\right)\left(P_2^\Omega + \sum_{\Theta_q=1}^6 P_2^{\Theta_q}\right)\Big|_{s=h_{c1}} \quad A_{mn}F_{m_t n_t l_t} \\[2ex] + \left(\Phi^M + \sum_{N_q=1}^2 \Phi^{N_q}\right)\left(P_2^\Omega + \sum_{\Theta_q=1}^6 P_2^{\Theta_q}\right)\Big|_{s=h_{c1}} \quad B_{mn}F_{m_t n_t l_t} \\[2ex] + \left(\Phi^M + \sum_{N_q=1}^2 \Phi^{N_q}\right)\left(P_2^\Omega + \sum_{\Theta_q=1}^6 P_2^{\Theta_q}\right)\Big|_{s=h_{c1}} \quad C_{mn}F_{m_t n_t l_t} \\[2ex] + \frac{h_p}{2}\left(\Phi^M + \sum_{N_q=1}^2 \Phi^{N_q}\right)\left(P_2^\Omega + \sum_{\Theta_q=1}^6 P_2^{\Theta_q}\right)\Big|_{s=h_{c1}} \quad D_{mn}F_{m_t n_t l_t} \\[2ex] + \frac{h_p}{2}\left(\Phi^M + \sum_{N_q=1}^2 \Phi^{N_q}\right)\left(P_2^\Omega + \sum_{\Theta_q=1}^6 P_2^{\Theta_q}\right)\Big|_{s=h_{c1}} \quad E_{mn}F_{m_t n_t l_t} \end{array} \right\} \tag{64}$$

$$|J_1| \cdot (r_1 + R_2) dr_1 d\theta_1$$

$$W_{P\&C_2} = \int_0^H \int_0^\vartheta \left\{ \begin{array}{l} \left(\Phi^M + \sum_{N_q=1}^2 \Phi^{N_q}\right)\left(P_2^\Omega + \sum_{\Theta_q=1}^6 P_2^{\Theta_q}\right)\Big|_{s=0} \quad A_{mn}G_{m_t n_t l_t} \\[2ex] + \left(\Phi^M + \sum_{N_q=1}^2 \Phi^{N_q}\right)\left(P_2^\Omega + \sum_{\Theta_q=1}^6 P_2^{\Theta_q}\right)\Big|_{s=0} \quad B_{mn}G_{m_t n_t l_t} \\[2ex] + \left(\Phi^M + \sum_{N_q=1}^2 \Phi^{N_q}\right)\left(P_2^\Omega + \sum_{\Theta_q=1}^6 P_2^{\Theta_q}\right)\Big|_{s=0} \quad C_{mn}G_{m_t n_t l_t} \\[2ex] + \frac{h_p}{2}\left(\Phi^M + \sum_{N_q=1}^2 \Phi^{N_q}\right)\left(P_2^\Omega + \sum_{\Theta_q=1}^6 P_2^{\Theta_q}\right)\Big|_{s=0} \quad D_{mn}G_{m_t n_t l_t} \\[2ex] + \frac{h_p}{2}\left(\Phi^M + \sum_{N_q=1}^2 \Phi^{N_q}\right)\left(P_2^\Omega + \sum_{\Theta_q=1}^6 P_2^{\Theta_q}\right)\Big|_{s=0} \quad E_{mn}G_{m_t n_t l_t} \end{array} \right\} \tag{65}$$

$$|J_2| \cdot (r_2 + R_2) dr_2 d\theta_2$$

The expressions of the work W_F done by the harmonic point force F on the composite laminated plate and the work W_F done by the monopole point sound source Q in the nth acoustic cavity in the coupled systems are as follows:

$$W_F = \iint_S \left\{ \left(\begin{array}{c} f_u A_{mn} + f_v B_{mn} + f_w C_{mn} \\ + f_{\phi_r} D_{mn} + f_{\phi_\theta} E_{mn} \end{array}\right)\left(\Phi^M + \sum_{N_q=1}^2 \Phi^{N_q}\right) \right\} r dr d\theta \tag{66}$$

$$f_i = F\delta(r - r_0)\delta(\theta - \theta_0) \tag{67}$$

$$W_{Q_1} = -\frac{1}{j\omega} \int_0^{L_{\alpha_1}} \int_0^{L_{\beta_1}} \int_0^{L_{z_1}} \left\{ \left(\mathbf{P}_1^{\Omega} + \sum_{\Theta_q=1}^{6} \mathbf{P}_1^{\Theta_q} \right) Q_s^1 \mathbf{F}_{m_t n_t l_t} \right\} \cdot |J_1| \cdot H_{\alpha_1} H_{\beta_1} H_{z_1} d\alpha_1 d\beta_1 dz_1 \quad (68)$$

$$W_{Q_2} = -\frac{1}{j\omega} \int_0^{L_{\alpha_2}} \int_0^{L_{\beta_2}} \int_0^{L_{z_2}} \left\{ \left(\mathbf{P}_2^{\Omega} + \sum_{\Theta_q=1}^{6} \mathbf{P}_2^{\Theta_q} \right) Q_s^2 \mathbf{G}_{m_t n_t l_t} \right\} \cdot |J_2| \cdot H_{\alpha_2} H_{\beta_2} H_{z_2} d\alpha_2 d\beta_2 dz_2 \quad (69)$$

$$Q_s^n = \frac{4\pi A}{j\rho_{C_n} c_n k} \delta_c(r - r_e)\delta_c(\theta - \theta_e)\delta_c(s - s_e) \quad (70)$$

where f_i ($i = u_j, v_j, w_j$) is the function of external load distribution, and the action position of harmonic point force F is (r_0, θ_0). Q_s^n represents the distribution function of the point sound source acting on the nth cavity, the amplitude of the point sound source is A (kg/s^2) and the specific position of the point sound source Q is (r_e, θ_e, s_e). δ and δ_c are two-dimensional and three-dimensional Dirac functions.

Each energy equation is substituted into Equations (41)–(43). According to Rayleigh–Ritz method, the partial derivatives of the unknown two-dimensional and three-dimensional Fourier coefficients are obtained in the Lagrange equation, and the results are equal to zero:

$$\frac{\partial L_P}{\partial \mathbf{P}_{mn}} = \frac{\partial T_P}{\partial \mathbf{P}_{mn}} - \frac{\partial U_P}{\partial \mathbf{P}_{mn}} - \frac{\partial U_{P-coupling}}{\partial \mathbf{P}_{mn}} - \frac{\partial U_{SP}}{\partial \mathbf{P}_{mn}} - \frac{\partial W_{P\&C_1}}{\partial \mathbf{P}_{mn}} - \frac{\partial W_{P\&C_2}}{\partial \mathbf{P}_{mn}} + \frac{\partial W_F}{\partial \mathbf{P}_{mn}} = 0 \quad (71)$$

$$\frac{\partial L_{C_1}}{\partial \mathbf{F}_{m_t n_t l_t}} = \frac{\partial T_{C_1}}{\partial \mathbf{F}_{m_t n_t l_t}} - \frac{\partial U_{C_1}}{\partial \mathbf{F}_{m_t n_t l_t}} - \frac{\partial U_{C_1-coupling}}{\partial \mathbf{F}_{m_t n_t l_t}} - \frac{\partial W_{P\&C_1}}{\partial \mathbf{F}_{m_t n_t l_t}} - \frac{\partial W_{C_1\&C_2}}{\partial \mathbf{F}_{m_t n_t l_t}} + \frac{\partial W_{C_1-wall}}{\partial \mathbf{F}_{m_t n_t l_t}} + \frac{\partial W_{Q_1}}{\partial \mathbf{F}_{m_t n_t l_t}} = 0 \quad (72)$$

$$\frac{\partial L_{C_2}}{\partial \mathbf{G}_{m_t n_t l_t}} = \frac{\partial T_{C_2}}{\partial \mathbf{G}_{m_t n_t l_t}} - \frac{\partial U_{C_2}}{\partial \mathbf{G}_{m_t n_t l_t}} - \frac{\partial U_{C_2-coupling}}{\partial \mathbf{G}_{m_t n_t l_t}} - \frac{\partial W_{P\&C_2}}{\partial \mathbf{G}_{m_t n_t l_t}} - \frac{\partial W_{C_2\&C_1}}{\partial \mathbf{G}_{m_t n_t l_t}} + \frac{\partial W_{C_2-wall}}{\partial \mathbf{G}_{m_t n_t l_t}} + \frac{\partial W_{Q_2}}{\partial \mathbf{G}_{m_t n_t l_t}} = 0 \quad (73)$$

$$\mathbf{P}_{mn} = \begin{bmatrix} \mathbf{A}_{mn} & \mathbf{B}_{mn} & \mathbf{C}_{mn} & \mathbf{D}_{mn} & \mathbf{E}_{mn} \end{bmatrix}^T \quad (74)$$

Transform Equation (71)–(73) into matrix form:

$$(\mathbf{K}_p - \omega^2 \mathbf{M}_p)\mathbf{P}_{mn} + \mathbf{C}_{C_1\&P}\mathbf{F}_{m_t n_t l_t} - \mathbf{C}_{C_2\&P}\mathbf{G}_{m_t n_t l_t} = \mathbf{F} \quad (75)$$

$$(\mathbf{K}_{c_1} - \omega \mathbf{Z}_{c_1} - \omega^2 \mathbf{M}_{c_1})\mathbf{F}_{m_t n_t l_t} + \omega^2 \mathbf{C}_{P\&C_1}\mathbf{P}_{mn} + \mathbf{C}_{C_1\&C_2}\mathbf{G}_{m_t n_t l_t} = \mathbf{Q}_1 \quad (76)$$

$$(\mathbf{K}_{c_2} - \omega \mathbf{Z}_{c_2} - \omega^2 \mathbf{M}_{c_2})\mathbf{G}_{m_t n_t l_t} - \omega^2 \mathbf{C}_{P\&C_2}\mathbf{P}_{mn} + \mathbf{C}_{C_2\&C_1}\mathbf{F}_{m_t n_t l_t} = \mathbf{Q}_2 \quad (77)$$

in which $\mathbf{K}_p$ and $\mathbf{K}_{c_n}$ respectively represent the stiffness matrix of the rotary composite laminated plate and the nth acoustic cavity in the coupled systems, and $\mathbf{M}_p$, $\mathbf{M}_{c_n}$ are the mass matrices. The impedance matrix of the nth acoustic cavity in the coupled systems is denoted by $\mathbf{Z}_{c_n}$. $\mathbf{C}_{C_n\&P}$ is the vibro-acoustic coupling matrix between the nth cavity and the composite laminated plate in coupled systems, and $\mathbf{C}_{P\&C_n} = \mathbf{C}_{C_n\&P}$.

When $\mathbf{F}$ and $\mathbf{Q}_n$ are equal to zero, Equations (75)–(77) can be combined to obtain the natural frequency and mode solving equations of the coupled systems. To facilitate the solution, the equations need to be converted into linear equations for solving:

$$(\mathbf{R} - \omega \mathbf{S})\mathbf{G} = 0 \quad (78)$$

$$\mathbf{R} = \begin{bmatrix} 0 & \mathbf{K}_p & 0 & 0 & 0 & 0 \\ \mathbf{K}_p & 0 & \mathbf{C}_{C_1\&P} & 0 & -\mathbf{C}_{C_2\&P} & 0 \\ 0 & 0 & 0 & \mathbf{K}_{c_1} & 0 & 0 \\ 0 & 0 & \mathbf{K}_{c_1} & -\mathbf{Z}_{c_1} & \mathbf{C}_{C_1\&C_2} & 0 \\ 0 & 0 & 0 & 0 & 0 & \mathbf{K}_{c_2} \\ 0 & 0 & \mathbf{C}_{C_2\&C_1} & 0 & \mathbf{K}_{c_2} & -\mathbf{Z}_{c_2} \end{bmatrix} \tag{79}$$

$$\mathbf{S} = \begin{bmatrix} \mathbf{K}_p & 0 & 0 & 0 & 0 & 0 \\ 0 & \mathbf{M}_p & 0 & 0 & 0 & 0 \\ 0 & 0 & \mathbf{K}_{c_1} & 0 & 0 & 0 \\ 0 & -\mathbf{C}_{P\&C_1} & 0 & \mathbf{M}_{c_1} & 0 & 0 \\ 0 & 0 & 0 & 0 & \mathbf{K}_{c_2} & 0 \\ 0 & \mathbf{C}_{P\&C_2} & 0 & 0 & 0 & \mathbf{M}_{c_2} \end{bmatrix} \tag{80}$$

$$\mathbf{G} = \begin{bmatrix} \mathbf{P}_{mn} & \omega\mathbf{P}_{mn} & \mathbf{F}_{m_t n_t l_t} & \omega\mathbf{F}_{m_t n_t l_t} & \mathbf{G}_{m_t n_t l_t} & \omega\mathbf{G}_{m_t n_t l_t} \end{bmatrix}^{\mathrm{T}} \tag{81}$$

Finally, the eigen solution ω is the natural frequency of the coupled systems, and the eigenvector $\mathbf{G}$ is the corresponding mode. By substituting harmonic point force and monopole point sound source into Equations (78)–(81), the steady-state response of the coupled systems can be obtained.

3. Numerical discussion and result analysis

According to the unified analysis model of the conical–cylindrical acoustic cavity coupled system and rotary composite laminated plate and conical–cylindrical double cavities coupled system, numerical discussion and result analysis are carried out to further research the vibro-acoustic characteristics. This section mainly verifies the convergence and accuracy of the coupled system model, analyzes the influence factors on natural frequency of the coupled systems under free vibration and studies the steady-state response analysis of the coupled systems under the action of harmonic point force and point sound source excitation. In this section, the boundary conditions of the composite laminated plate in the coupled system are represented by artificial virtual spring boundary technology, which can simulate complex boundary conditions. The spring stiffness settings of each boundary condition are presented in Table 2. Table 3 shows the material parameters of the composite laminated plate in the examples. The acoustic medium of acoustic cavities is air, where the density of air is defined as $\rho_{air} = 1.21$ kg/m^3, and the speed at which sound waves travel through air is defined as $c_{air} = 340$ m/s.

3.1 Unified analysis model validation

The convergence analysis and accuracy verification of the model of the coupled systems established above will be carried out. Tables 4 and 5 demonstrate the first eight order natural

Table 2.
Boundary spring stiffness values corresponding to different boundary conditions

Boundary conditions	Boundary springs					Coupling springs				
	k_u	k_v	k_w	K_r	K_θ	k_{uc}	k_{vc}	k_{wc}	K_{rc}	$K_{\theta c}$
Free (F)	0	0	0	0	0	0	0	0	0	0
Simple (S)	5e11	5e11	5e11	0	0	5e11	5e11	5e11	0	0
Clamped (C)	5e11	5e11	5e11	5e11	5e11	5e11	5e11	5e11	5e11	5e11
Elastic 1 (E^1)	0	0	0	2.5e3	2.5e3	0	0	0	2.5e3	2.5e3
Elastic 2 (E^2)	1e6	1e6	1e6	1e6	1e6	1e6	1e6	1e6	1e6	1e6

frequencies of the coupled systems obtained by the proposed method with different truncation values, and the numerical results are compared with the FE simulation results. M_p and N_p are the truncation values of the laminated plate, and M_c, N_c and Q_c are the truncation values of acoustic cavities. The acoustic walls of cavities in this example are all rigid walls, and the boundary conditions of the rotary plate are set as C-C-C-C. The geometric parameters of the coupled systems in Tables 4 and 5 are as follows: $R_0 = 0.5$ m, $R_1 = 1$ m, $R_2 = 1.5$ m, $H = 0.5$ m, $\alpha = \pi/6$, $L_2 = 1.5$ m, $h_p = 0.02$ m, $\vartheta = \pi/2$. The material used is [Glass/epoxy | Boron/epoxy], and the layering angle is [0 |π/2]. It can be seen from Tables 4 and 5 that when $M_c \times N_c \times Q_c = 5 \times 5 \times 5$ and $M_p \times N_p = 10 \times 10$, the natural frequencies of each order basically complete convergence. In contrast to the FE simulation results, the maximum error of the natural frequency is less than 0.1%, indicating the accuracy of the proposed method. Therefore, it is reliable to select truncation values $M_c \times N_c \times Q_c = 5 \times 5 \times 5$ and $M_p \times N_p = 10 \times 10$ in the numerical calculation of present method.

When the rotation angle of the coupled systems $\vartheta = 2\pi$, the rotary composite laminated plate and acoustic cavities in the systems will generate additional coupling potential energy, exerting an influence on the vibro-acoustic characteristics of the systems. Therefore, the accuracy of the proposed method is verified again as shown in Table 6. The acoustic walls of cavities in this example are all rigid walls, and the boundary conditions of the rotary plate are set as S-S-S-S. The geometric parameters of the coupled systems in Table 6 are as follows: $R_0 = 0.7$ m, $R_1 = 1.4$ m, $R_2 = 2.1$ m, $H = 0.7$ m, $\alpha = \pi/6$, $L_2 = 2.5$ m, $h_p = 0.03$ m. The material used is [Glass/epoxy | Boron/epoxy | Glass/epoxy], and the layering angle is [π/4 | 0 |π/4]. The maximum error between the numerical calculation results and the FE simulation results in Table 6 is less than 1%, which indicates that present method still has well accuracy when the rotation angle $\vartheta = 2\pi$.

3.2 Free vibration analysis
In this section, the free vibration of the conical–cylindrical acoustic cavity coupled system and rotary composite laminated plate and conical–cylindrical double cavities coupled system is conducted to investigate the effects of related parameters on the vibro-acoustic characteristics of the coupled systems. Figure 5 shows the variations of natural frequencies of the coupled systems with different rotation angles. The acoustic walls of cavities in this example are all rigid walls, and the boundary conditions of the rotary plate are

Material	ρ_{plate} (kg/m^3)	E_1 (GPa)	E_2 (GPa)	G_{23} (GPa)	G_{12} (GPa)	G_{13} (GPa)	μ_{12}
				Elastic engineering constant			
Glass/epoxy	1,810	38.6	8.3	4.14	4.14	4.14	0.26
Boron/epoxy	2,000	204.0	18.3	5.5	5.5	5.5	0.23
Source(s): Ramkumar and Ganesan (2009)							

Table 3.
Material parameters applied for the plate in the numerical calculation

$M_c \times N_c \times Q_c$	1	2	3	4	5	6	7	8
				Mode number				
$3 \times 3 \times 3$	73.606	91.299	127.067	136.443	172.670	176.672	205.789	205.903
$4 \times 4 \times 4$	73.572	91.297	127.058	136.410	172.626	176.668	205.790	205.892
$5 \times 5 \times 5$	73.572	91.297	127.058	136.410	172.626	176.668	205.790	205.892
$6 \times 6 \times 6$	73.572	91.297	127.058	136.410	172.626	176.668	205.790	205.892
FEM	73.575	91.297	127.060	136.410	172.630	176.670	205.790	205.890

Table 4.
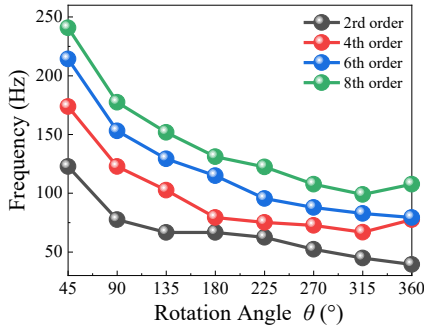Analysis of natural frequency convergence of conical–cylindrical acoustic cavity coupled system

$M_c \times N_c \times Q_c$	$M_p \times N_p$	Mode number							
		1	2	3	4	5	6	7	8
$3 \times 3 \times 3$	5×5	87.003	107.550	113.281	142.834	169.711	173.100	203.250	206.832
	6×6	87.003	107.549	113.280	142.833	169.710	173.098	203.250	206.827
	7×7	87.002	107.549	113.280	142.831	169.710	173.097	203.250	206.826
	8×8	87.002	107.549	113.279	142.830	169.710	173.097	203.249	206.826
	9×9	87.002	107.549	113.279	142.830	169.711	173.097	203.248	206.823
	10×10	87.002	107.549	113.279	142.829	169.711	173.096	203.249	206.826
$4 \times 4 \times 4$	5×5	87.002	107.549	113.279	142.829	169.704	173.096	203.249	206.822
	6×6	87.002	107.549	113.280	142.833	169.705	173.098	203.249	206.827
	7×7	87.002	107.549	113.280	142.831	169.705	173.097	203.249	206.825
	8×8	87.002	107.549	113.279	142.830	169.704	173.097	203.249	206.824
	9×9	87.002	107.549	113.279	142.830	169.704	173.096	203.249	206.822
	10×10	87.002	107.549	113.279	142.829	169.704	173.096	203.249	206.822
$5 \times 5 \times 5$	5×5	87.003	107.549	113.282	142.834	169.690	173.100	203.247	206.832
	6×6	87.003	107.549	113.280	142.833	169.688	173.098	203.247	206.827
	7×7	87.002	107.549	113.279	142.832	169.684	173.099	203.247	206.825
	8×8	87.002	107.549	113.279	142.830	169.689	173.097	203.247	206.830
	9×9	87.002	107.548	113.279	142.830	169.689	173.096	203.247	206.822
	10×10	87.002	107.548	113.279	142.829	169.688	173.096	203.247	206.822
	FEM	87.021	107.520	113.320	142.900	169.610	173.110	203.100	206.870

Table 5.
Analysis of natural frequency convergence of the rotary composite laminated plate and conical–cylindrical double cavities coupled system

set as S-S-C-C. The determined geometric parameters are as follows: $R_0 = 0.6$ m, $R_1 = 1.2$ m, $R_2 = 1.7$ m, $H = 0.5$ m, $\alpha = \pi/4$, $L_2 = 2$m, $h_p = 0.024$ m. The material used is [Glass/epoxy | Boron/epoxy], and the layering angle is $[-\pi/4 \ |\pi/4]$. As shown in Figure 5, the natural frequency of the same order decrease with the increase of rotation angle ϑ. However, the situation changes when the rotation angle $\vartheta = 2\pi$. Taking the rotary composite laminated plate and conical–cylindrical double cavities coupled system as an instance, Table 7 gives the first eight natural frequencies of the coupled system with various rotation angles. It can be found from Table 7 that the natural frequency at $\vartheta = 2\pi$ is basically the same as that at $\vartheta = \pi$. In the case of coupling of the two acoustic walls, a closed loop will be formed, and repeated modes will be generated, resulting in continuous expansion of the natural frequencies of each order. These conditions explain why the natural frequency rises again when $\vartheta = 2\pi$ in Figure 5.

System type	Method	Mode number							
		1	2	3	4	5	6	7	8
Cone–cylinder	Present	33.182	33.182	47.200	59.918	59.918	64.703	64.703	86.115
	FEM	33.183	33.183	47.204	59.920	59.920	64.701	64.701	86.118
Cone–plate–cylinder	Present	31.081	31.311	39.149	39.152	62.059	66.339	67.719	74.426
	FEM	31.074	31.100	39.066	39.170	62.034	62.091	67.690	73.946

(a) The conical-cylindrical acoustic cavity coupled system

(b) The rotary composite laminated plate and conical-cylindrical double cavities coupled system

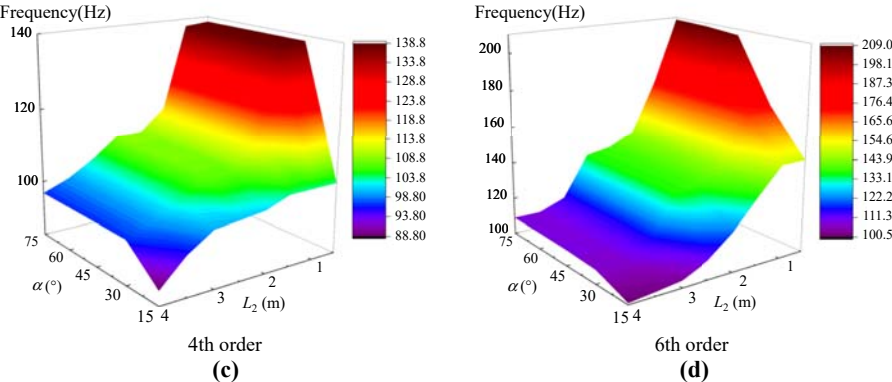| ϑ	Mode number							
	1	2	3	4	5	6	7	8
$\pi/4$	84.953	149.439	169.809	171.897	180.560	193.876	223.370	226.293
$\pi/2$	74.921	84.917	94.274	113.247	149.379	169.133	171.665	180.493
$3\pi/4$	49.971	63.493	84.906	98.525	99.807	124.060	130.987	149.368
π	37.484	47.798	74.907	84.901	92.815	94.270	112.224	113.199
$5\pi/4$	29.986	38.305	59.949	75.919	84.897	89.848	90.051	103.915
$3\pi/2$	24.995	31.956	49.966	63.492	74.908	84.892	88.509	94.267
$7\pi/4$	21.429	27.402	42.826	54.561	64.223	81.189	84.894	85.581
2π	37.478	37.626	47.795	47.904	74.897	79.243	84.880	92.769

For the conical–cylindrical acoustic cavity coupled system and rotary composite laminated plate and conical–cylindrical double cavities coupled system, it is necessary to analyze the effects of conical cavity cone-apex angle α and cylindrical cavity height L_2 on the natural frequency of the coupled systems. The variations of natural frequencies of the coupled systems with different cone-apex angle α and height L_2 are presented in Figure 6. The acoustic walls of cavities in this example are all rigid walls, and the boundary conditions of the rotary plate are set as S-S-C-C. The determined geometric parameters are as follows: $R_0 = 0.5$ m, $R_1 = 1$m, $R_2 = 1.5$ m, $H = 0.5$ m, $\vartheta = \pi/2$, $h_p = 0.018$ m. The material used is [Glass/epoxy | Boron/epoxy], and the layering angle is $[-\pi/2 \,|\, \pi/2]$. As can be seen from Figure 6, the natural frequency of the coupled system degrades with the decrease of cone-apex angle α and the increase of height L_2.

Compared with the conical–cylindrical acoustic cavity coupled system, the rotary composite laminated plate and conical–cylindrical double cavities coupled system is also affected by the relevant parameters of the composite laminated plate. The first eight natural frequencies of the coupled system under different boundary conditions are shown in Table 8. The acoustic walls of cavities in this example are all rigid walls. The geometric parameters of the coupled system in Table 8 are as follows: $R_0 = 0.5$ m, $R_1 = 1$m, $R_2 = 1.5$ m, $H = 0.5$ m, $\alpha = \pi/6$, $L_2 = 1.5$ m, $h_p = 0.02$ m, $\vartheta = \pi/2$. The material used is [Glass/epoxy | Boron/epoxy], and the layering angle is $[0 \,|\, \pi/2]$. It can be found from Table 8 that the natural frequency of the coupled system calculated by present method is basically consistent with the FE simulation

The conical-cylindrical acoustic cavity coupled system

The rotary composite laminated plate and conical-cylindrical double cavities coupled system

Figure 6.
The surface diagram of the natural frequency of the coupled systems with different height L_2 and cone-apex angle α

results with different boundary conditions, which again proves the accuracy of the proposed method. Meanwhile, the natural frequency of the coupled system increases with the increase of the stiffness value of boundary springs, and the calculation results of elastic boundary 1 (E^1) and elastic boundary 2 (E^2) also verify the reliability of this conclusion.

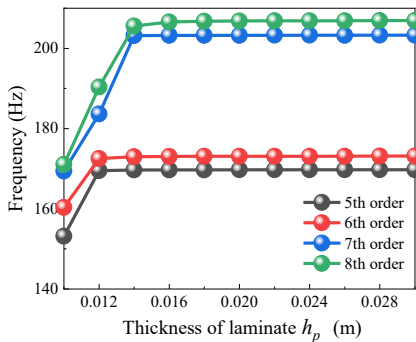Besides boundary conditions, the thickness of the plate is also necessary to be studied parameterized. Figure 7 shows the influence trend of laminated plate thickness h_p on the natural frequency of the coupled system with different size conditions. The acoustic walls of cavities in this example are all rigid walls, and the boundary conditions of the rotary composite laminated plate are set as C-C-C-C. The determined geometric parameters are as follows: $\alpha = \pi/6, L_2 = 1.5$ m, $\vartheta = \pi/2$. The material used is [Glass/epoxy | Boron/epoxy], and the layering angle is [0 |$\pi/2$]. As can be seen from Figure 7, the natural frequency of the coupled system shows an upward trend with the increase of h_p.
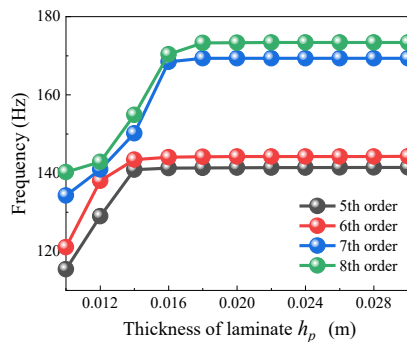
3.3 Steady state response analysis

In this section, the displacement response and sound pressure response of the conical–cylindrical acoustic cavity coupled system and rotary composite laminated plate and conical–cylindrical double cavities coupled system under the excitation of point sound source are researched. Figures 8 and 9 demonstrate the displacement and sound pressure response curves of the coupled systems under monopole point sound source excitation at various

Boundary conditions	Method	1	2	3	Mode number 4	5	6	7	8
FSFS	Present	18.331	49.650	86.875	93.362	107.675	113.762	143.158	159.908
	FEM	19.886	51.845	87.101	95.609	108.430	113.720	143.210	157.040
FCFC	Present	55.957	83.038	87.549	107.606	113.702	129.403	143.319	169.696
	FEM	55.560	83.867	88.011	107.970	113.710	131.490	143.390	169.960
SCSF	Present	86.974	107.536	113.191	142.690	169.688	172.991	203.186	206.154
	FEM	87.005	107.450	113.260	143.830	169.340	173.060	202.680	206.700
SCSC	Present	86.986	107.541	113.211	142.753	169.693	173.034	203.211	206.379
	FEM	87.009	107.470	113.260	143.850	169.360	173.070	202.730	206.730
CCCC	Present	87.002	107.549	113.279	142.829	169.704	173.096	203.249	206.822
	FEM	87.021	107.520	113.320	142.900	169.610	173.110	203.100	206.870
$E^1E^1E^1E^1$	Present	15.273	27.781	32.861	61.821	77.825	87.728	107.738	113.822
$E^2E^2E^2E^2$	Present	35.894	58.401	66.374	82.787	87.768	106.134	107.745	114.854

Table 8.
Analysis of the influence of different boundary conditions on the rotary composite laminated plate and conical–cylindrical double cavities coupled system

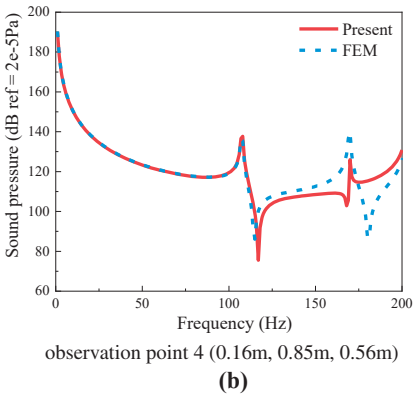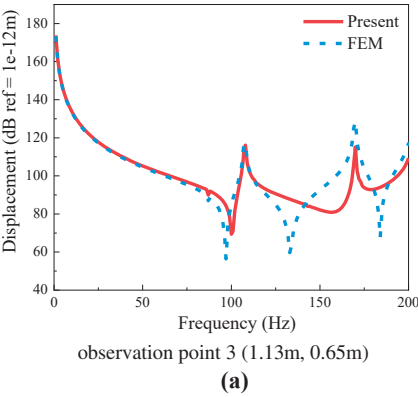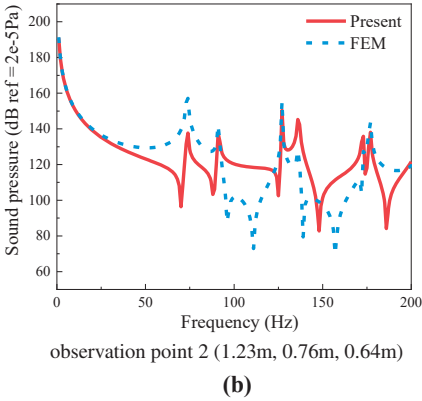$R_0 = 0.5$m, $R_1 = 1$m, $R_2 = 1.5$m, $H = 0.5$m
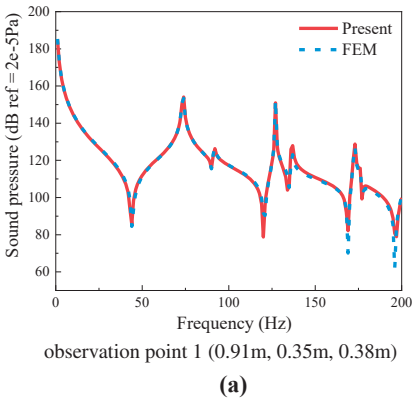
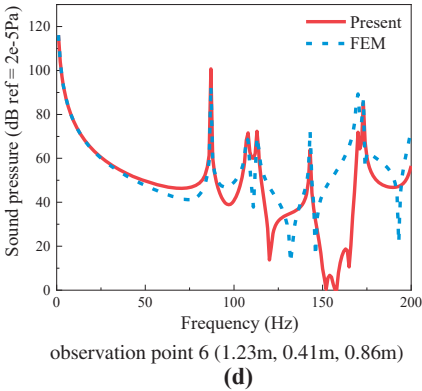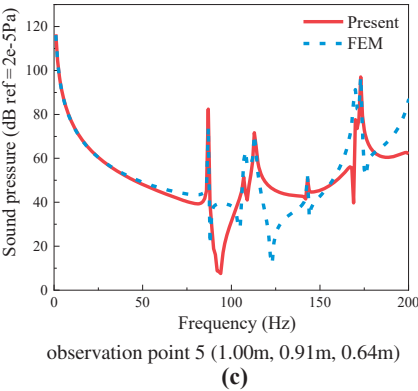(a)

$R_0 = 0.6$m, $R_1 = 1.2$m, $R_2 = 1.8$m, $H = 0.6$m

(b)

Figure 7.
The variation curve of the natural frequency of the rotary composite laminated plate and conical–cylindrical double cavities coupled system with different thickness h_p

observation points. The acoustic walls, boundary condition, geometric parameters, materials used and layering angle of the coupled systems are consistent with those in Tables 4 and 5. The action position of point sound source is at (0.77 , 0.69, 0.29 m) in cavity 1, observation point 1 is located at (0.91 , 0.35, 0.38 m) in cavity 1, observation point 2 is located at (1.35 , 0.38, 0.48 m) in cavity 2, observation point 3 is located at (1.13 m, 0.65 m) on the surface of

Figure 8.
The sound pressure response curves of the conical–cylindrical acoustic cavity coupled system with the excitation of a point source

observation point 1 (0.91m, 0.35m, 0.38m)

(a)

observation point 2 (1.23m, 0.76m, 0.64m)

(b)

observation point 3 (1.13m, 0.65m)

(a)

observation point 4 (0.16m, 0.85m, 0.56m)

(b)

Figure 9.
The displacement and sound pressure response curves of the rotary composite laminated plate and conical–cylindrical double cavities coupled system with the excitation of a point source

observation point 5 (1.00m, 0.91m, 0.64m)

(c)
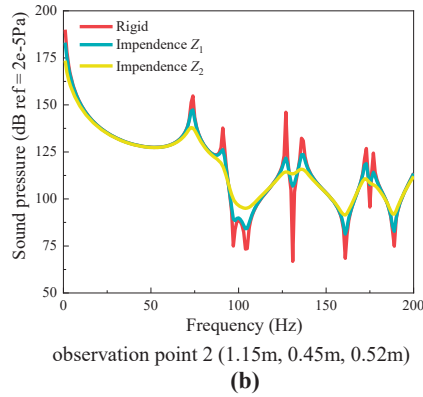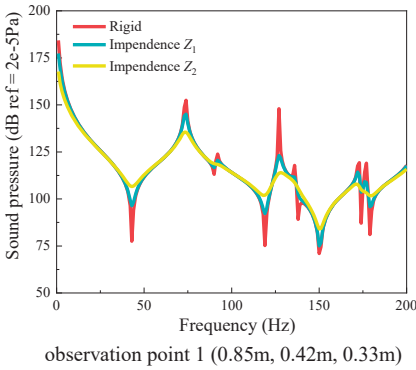
observation point 6 (1.23m, 0.41m, 0.86m)

(d)

composite laminated plate, observation point 4 is located at (0.16 , 0.85, 0.56 m) in cavity 1, observation point 5 is located at (1.00 , 0.91, 0.64 m) in cavity 2 and observation point 6 is located at (1.23 , 0.41, 0.86 m) in cavity 2. It can be seen from Figures 8 and 9 that the response curve obtained by the proposed method is consistent with the results of FE simulation, which proves the accuracy of the displacement and sound pressure response analysis model of the coupled systems under the excitation of point sound source.
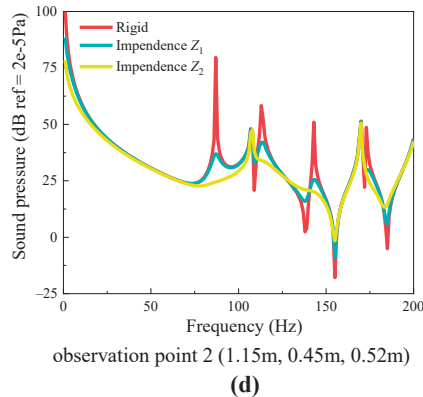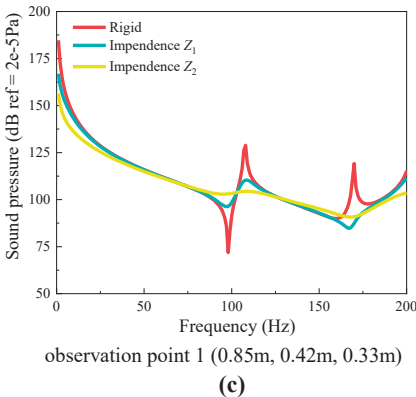
The sound pressure response of the coupled systems under the excitation of a point sound source with different impedance value of the acoustic walls is presented in Figure 10. All the six acoustic walls in the coupled systems are impedance walls, and the impedance values of the acoustic walls are rigid, $Z_1 = \rho_c c_0 (100 - j)$ and $Z_2 = \rho_c c_0 (30 - j)$. The boundary condition, geometric parameters, materials used and layering angle of the coupled systems are consistent with those in Tables 4 and 5. The action position of point sound source is at (0.80 , 0.71, 0.25 m) in cavity 1, observation point 1 is located at (0.85 , 0.42, 0.33 m) in cavity 1 and observation point 2 is located at (1.15 , 0.45, 0.52 m) in cavity 2.

As shown in Figure 10, the amplitude of the sound pressure response is reduced, and the effect of resonance suppression is achieved when the acoustic wall is changed to the impedance wall, whose influence increases with the increase of the impedance value. However, the variation of acoustic walls in the coupled systems does not affect the waveform of the response.

The conical-cylindrical acoustic cavity coupled system

observation point 1 (0.85m, 0.42m, 0.33m)
(a)

observation point 2 (1.15m, 0.45m, 0.52m)
(b)

The rotary composite laminated plate and conical-cylindrical double cavities coupled system

observation point 1 (0.85m, 0.42m, 0.33m)
(c)

observation point 2 (1.15m, 0.45m, 0.52m)
(d)

Figure 10.
Sound pressure
response curves of the
coupled systems under
the excitation of a point
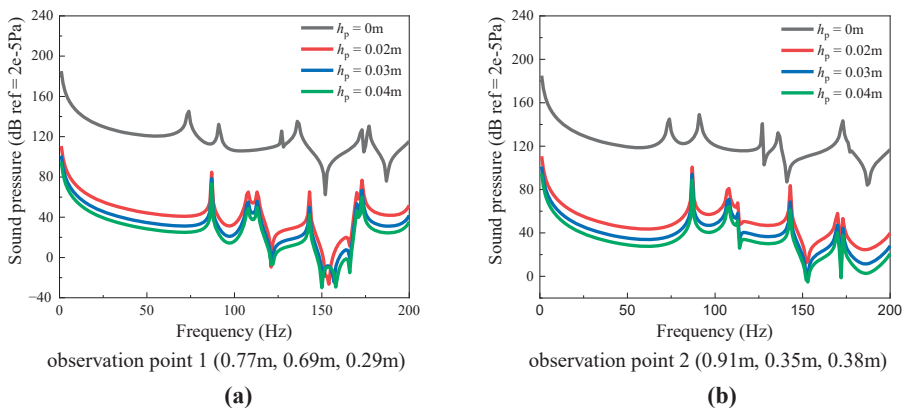source with different
impedance value of the
acoustic walls

In the rotary composite laminated plate and conical–cylindrical double cavities coupled system, if the point source excitation and the observation point are not in the same cavity, the sound pressure response of the coupled system will be affected by the laminated plate between the two cavities. To investigate the influence mechanism on the thickness of plate, Figure 11 gives the sound pressure response curves of the observation points in the upper conical cavity under the excitation of the point sound source in the lower cylindrical cavity with different thicknesses of the laminated plate, where $h_p = 0$ m denotes that there is no plate between the two acoustic cavities, and the system is cylindrical-conical acoustic cavity coupled system. The acoustic walls, boundary condition, geometric parameters, materials used and layering angle of the coupled systems are consistent with those in Tables 4 and 5. The action position of point sound source is at (1.23 , 0.41, 0.86 m) in cavity 2, observation point 1 is located at (0.77 , 0.69, 0.29 m) in cavity 1 and observation point 2 is located at (0.91 , 0.35, 0.38 m) in cavity 1. It is not difficult to know from Figure 11 that the amplitude of sound pressure response curves at the same observation point decreases with the increase of the plate thickness, especially the difference between the sound pressure response and the sound pressure response of the composite laminated plate is apparent. The results show that the composite laminated plate in the coupled system has an impact on the noise reduction, and the effect increases with the increase of the thickness of composite laminated plate.

4. Conclusion
A unified analysis model of the rotary composite laminated plate and conical–cylindrical double cavities coupled system is constructed in this investigation. First, the admissible displacement and sound pressure functions of the rotary laminated plate and acoustic cavity are presented. Second, the energy functional of the laminated plate structure domain and cavity sound field domain is proposed. Then, the coupling potential energy between the cavities and the plate-double cavities is introduced to obtain the total energy functional of the coupled systems. Finally, the energy functional is solved by the Rayleigh–Ritz method. The free vibration and steady-state response of the coupled systems are studied by the numerical results of examples, and the following significant conclusions are obtained:

(1) The unified analysis model established in this paper has good convergence and accuracy when the truncation values $M_c \times N_c \times Q_c = 5 \times 5 \times 5$ and $M_p \times N_p = 10 \times 10$.

(2) Under the condition of free vibration, the natural frequency of the rotary composite laminated plate and conical–cylindrical double cavities coupled system increases

Figure 11.
The effect of different thickness h_p on the sound pressure response with the excitation of point sound source in the coupled system

with the increase of the rotation angle, the spring stiffness, thickness of the plate and cone-apex angle of the conical acoustic cavity. It decreases with the height of the cylindrical acoustic cavity increasing.

(3) In the conical–cylindrical acoustic cavity coupled system and rotary composite laminated plate and conical–cylindrical double cavities coupled system, the impedance wall can reduce the amplitude of the sound pressure response and suppress the resonance of the coupled systems. The effect of the impedance wall increases with the increase of the impedance value but has no effect on the waveform of the response. In the rotary composite laminated plate and conical–cylindrical double cavities coupled system, the composite laminated plate has a good noise reduction effect and increases with the increase of the plate thickness.

References

Birk, C., Liu, L. and Song, C. (2016), "Coupled acoustic response of two-dimensional bounded and unbounded domains using doubly-asymptotic open boundaries", *Journal of Computational Physics*, Vol. 310, pp. 252-284.

Carrera, E., Cinefra, M. and Li, G. (2018), "Refined finite element solutions for anisotropic laminated plates", *Composite Structures*, Vol. 183, pp. 63-76.

Chen, Y., Jin, G. and Liu, Z. (2017), "A domain decomposition method for analyzing a coupling between multiple acoustical spaces (L)", *The Journal of the Acoustical Society of America*, Vol. 141 No. 5, pp. 3018-3021.

Cinefra, M., Moruzzi, M.C., Bagassi, S., Zappino, E. and Carrera, E. (2021), "Vibro-acoustic analysis of composite plate-cavity systems via CUF finite elements", *Composite Structures*, Vol. 259, 113428.

De Rosa, S., Franco, F., Li, X. and Polito, T. (2012), "A similitude for structural acoustic enclosures", *Mechanical Systems and Signal Processing*, Vol. 30, pp. 330-342.

Ferreira, A., Carrera, E., Cinefra, M., Viola, E., Tornabene, F., Fantuzzi, N. and Zenkour, A.M. (2014), "Analysis of thick isotropic and cross-ply laminated plates by generalized differential quadrature method and a unified formulation", *Composites Part B: Engineering*, Vol. 58, pp. 544-552.

Larbi, W., Deü, J.-F. and Ohayon, R. (2012), "Finite element formulation of smart piezoelectric composite plates coupled with acoustic fluid", *Composite Structures*, Vol. 94 No. 2, pp. 501-509.

Moores, B.A., Sletten, L.R., Viennot, J.J. and Lehnert, K.W. (2018), "Cavity quantum acoustic device in the multimode strong coupling regime", *Physical Review Letters*, Vol. 120 No. 22, p. 5, 227701.

Ramkumar, K. and Ganesan, N. (2009), "Vibration and damping of composite sandwich box column with viscoelastic/electrorheological fluid core and performance comparison", *Materials and Design*, Vol. 30 No. 8, pp. 2981-2994.

Sarigül, A. and Karagözlü, E. (2014), "Vibro-acoustic analysis of composite plates", *Journal of Physics: Conference Series*, IOP Publishing, Vol. 490, 012212.

Sarıgül, A.S. and Karagözlü, E. (2018), "Vibro-acoustic coupling in composite plate-cavity systems", *Journal of Vibration and Control*, Vol. 24 No. 11, pp. 2274-2283.

Shi, S., Jin, G., Xiao, B. and Liu, Z. (2018), "Acoustic modeling and eigenanalysis of coupled rooms with a transparent coupling aperture of variable size", *Journal of Sound and Vibration*, Vol. 419, pp. 352-366.

Shu, L., Wang, M.Y. and Ma, Z. (2014), "Level set based topology optimization of vibrating structures for coupled acoustic–structural dynamics", *Computers and Structures*, Vol. 132, pp. 34-42.

Tanaka, N., Takara, Y. and Iwamoto, H. (2012), "Eigenpairs of a coupled rectangular cavity and its fundamental properties", *The Journal of the Acoustical Society of America*, Vol. 131 No. 3, pp. 1910-1921.

Unnikrishnan Nair, S., Shete, C.D., Subramoniam, A., Handoo, K.L. and Padmanabhan, C. (2010), "Experimental and computational investigation of coupled resonator–cavity systems", *Applied Acoustics*, Vol. 71 No. 1, pp. 61-67.

Van Genechten, B., Vandepitte, D. and Desmet, W. (2011), "A direct hybrid finite element – wave based modelling technique for efficient coupled vibro-acoustic analysis", *Computer Methods in Applied Mechanics and Engineering*, Vol. 200 No. 5, pp. 742-764.

Wang, G., Cui, X.Y., Liang, Z.M. and Li, G.Y. (2015), "A coupled smoothed finite element method (S-FEM) for structural-acoustic analysis of shells", *Engineering Analysis with Boundary Elements*, Vol. 61, pp. 207-217.

Zhang, P., Fei, Q.G., Wu, S.Q. and Li, Y.B. (2016), "A dimensionless quotient for determining coupling strength in modal energy analysis", *Journal of Vibration and Acoustics*, Vol. 138 No. 6, 061014.

Zhang, H., Zhu, R.P., Shi, D.Y. and Wang, Q.S. (2019), "A simplified plate theory for vibration analysis of composite laminated sector, annular and circular plate", *Thin-Walled Structures*, Vol. 143, 106252.

Zhang, H., Zhu, R.P., Shi, D.Y. and Wang, Q.S. (2020a), "A unified modeling method for the rotary enclosed acoustic cavity", *Applied Acoustics*, Vol. 163, 107230.

Zhang, H., Zhu, R.P., Shi, D.Y., Wang, Q.S. and Yu, H.L. (2020b), "Study on vibro-acoustic property of composite laminated rotary plate-cavity system based on a simplified plate theory and experimental method", *International Journal of Mechanical Sciences*, Vol. 167, 105264.

Corresponding author
Hong Zhang can be contacted at: zhanghong@nuaa.edu.cn